An Assessment of Present and Historical (1984-2012) Lake Diefenbaker Water Clarity and Chlorophyll-*a* Concentration Using Landsat Imagery

A Thesis Submitted to the College of Graduate Studies and Research in Partial Fulfillment of the Requirements for the Degree of Master of Science

Department of Biology

University of Saskatchewan

By

Hayden D. Yip

Copyright Statement:

'I hereby grant to University of Saskatchewan and/or its agents the non-exclusive license to archive and make accessible, under the conditions specified below, my thesis, dissertation, or project report in whole or in part in all forms of media, now or for the duration of my copyright ownership. I retain all other ownership rights to the copyright of the thesis, dissertation or project report. I also reserve the right to use in future works (such as articles or books) all or part of this thesis, dissertation, or project report.

I hereby certify that, if appropriate, I have obtained permission from the owner(s) of each third party copyrighted matter that is included in my thesis, dissertation, or project report, allowing distribution as specified below. I certify that the version I submitted is the same as that approved by my advisory committee.'

Abstract: The use of earth observing satellites can be an effective supplement or alternative to traditional field sampling. The Landsat series of satellites have been particularity useful in assessing water quality in lakes, oceans, and reservoirs. This study utilized Landsat 5 and 7 imagery to model Secchi disk depth (SDD) and chlorophyll-*a* concentrations (Chl-*a*) at Lake Diefenbaker, Saskatchewan. I used data from these Landsat satellites to answer the following questions: First, can models that predict water quality (SDD and Chl-*a* concentration) be developed for Lake Diefenbaker using Landsat imagery? Second, can these models identify trends that have taken place at the reservoir from 1984-2012? Third, can I determine if ephemeral events like algal blooms or flooding have an effect on the reservoir? Novel models were developed from data collected in 2011 and 2012 that could predict SDD and Chl-*a* concentrations in the reservoir (linear regression, model I). These models explain less variation than comparable studies, but the loss in explanatory power is made up by their ability to predict data from any Landsat image of the reservoir. My study showed that predicted SDD and Chl-*a* concentration were positively related, an atypical relationship in freshwater systems. During the archive study period (1984-2012), both mean seasonal SDD and mean seasonal Chl-*a* have significantly decreased throughout the reservoir ($p<0.05$, regime-shift analysis). Spatially, the greatest decrease in SDD was closest to the major inflow the SSR, while downstream areas in the reservoir have decreased minimally. There was a decline in Chl-*a* concentrations that was spatially consistent throughout the reservoir. There was a significant negative relationship between flow rate and both water clarity and Chl-*a* concentrations ($P<0.05$, model II linear regression). Algal blooms occurred sporadically throughout the study period. There were blooms in 9% of images analyzed. Blooms typically occurred in the Qu'Appelle arm of the

reservoir in the late summer and fall. The water quality data extracted by this study can be useful to many future studies, as historical data is absent for much of the reservoir's history.

Acknowledgments: There are a number of people whose contributions to the research contained in this thesis were invaluable. First and foremost, I'd like to thank my supervisor, Dr. Jeff Hudson, and my committee members, Dr. Xulin Guo and Dr. Phil McLoughlin. The expertise and guidance these people provided was critical in allowing me to finish my research. Without their advice, this work could not have been completed. I would also like to thank two anonymous reviewers that contributed comments regarding chapter 3 of this manuscript.

The students and technicians in the laboratory, Kristine Hunter, Jessica Johansson, Chance Prestie, Kerry Head, Oghenemise Abirhire, and David Vandergucht, also deserve recognition. Many of these people provided field assistance, but were also great friends and advisors. In addition, I would like to thank Dr. Jeff Sereda and Dr. Rebecca North for their advice and contributions. I would also like to thank the seasonal technicians in the Limnology Laboratory, Torben Brydges, Tom Perry, Sheena McInnes, and Laurie Johnson for their hard work. Two anonymous reviewers also gave extremely useful comments that improved the third chapter of this manuscript. My friends in the department and those outside of it also deserve thanks for keeping me entertained and distracted for the duration of my studies. Lastly, I would like to thank my partner, Tara Richardson. Her help editing and reviewing my writing, as well as providing moral support was incredibly important.

I also owe thanks to Dr. Howard Wheater, Dr. Jeff Hudson, the Global Institute for Water Security, the University of Saskatchewan, and the Department of Biology for financial and technical support for my degree.

Table of Contents

List of Tables:

Chapter 1:

Chapter 2:

Chapter 3:

List of Figures

Chapter 1:

Chapter 2:

Chapter 3:

Chapter 1: Introduction:

1.1 Water quality, Eutrophication, and Algal Blooms

Threats to water security and water quality are becoming increasingly prevalent due to human population growth and economic development (Vörösmarty et al. 2010). Anthropogenic activities such as agriculture, industrial development, and municipal growth contribute to the use of large quantities of water (Malmqvist and Rundle 2002). The economic cost of water pollution has already been high, with multi-billion dollar damages reported in the United States (Dodds et al. 2008). Water pollution can thus have negative repercussions regarding economic stability, public health, and potential damage to the natural environment.

Nutrients can enter a water body through both point and non-point sources. Point sources would include a sewage treatment plant (Jarvie et al. 2006), an aquaculture facility, or heavy metal pollution from industry in the Laurentian Great Lakes region (Nriagu et al. 1979). Non-point sources might include agricultural runoff (Gober and Wheater 2014), atmospheric deposition (Baron et al. 2011; Jassby et al. 1994), or shoreline erosion (Boynton et al. 1995). Non-point source pollution, such as agricultural run-off is much more difficult to control. Nutrients such as nitrogen and phosphorous can often cause eutrophication. The uptake of these nutrients by algae can lead to rapid increases in algal biomass, commonly known as algal blooms. Inputs of these nutrients have been directly linked to the increasing prevalence of algal blooms (Paerl 2008; Sellner et al. 2003). This phenomenon was demonstrated by phosphorous fertilization in the Experimental Lakes Area in Ontario, Canada (Schindler 1974). Unnaturally high algal biomass can detrimentally affect a lake in a number of ways. First, Algal blooms can also make lakes less attractive for human use (Dyson and Huppert 2010). Blooms

are often reported as having a foul odor and giving water a poor taste (Paerl 2008). Many species of algae will also produce toxins that are potentially damaging to organisms that live within or consume the water of an affected lake (Landsberg 2002). The blue-green algae (cyanobacteria) are particularly dangerous because some species can produce powerful neurotoxins (Carmichael 2001). Fish kills that are caused by the toxins produced by the algae can be particularly damaging to an entire aquatic ecosystem (Kangur et al. 2005). Cyanobacterial blooms have also been occasionally linked to livestock and other animal deaths caused by microcystin toxins (Straubinger-Gansberger 2014; Mez et al. 1997). Therefore, it is clear that monitoring the health of our water resources has become of critical importance to ensure both the safety of the human population and the preservation of the natural environment.

1.2 Water Quality Monitoring Techniques

Water quality can be monitored in a number of different ways. Traditional sampling and monitoring of lakes take place *in situ*, and requires sampling to either take place in the lake or for water to be brought to a laboratory for analysis. There are many organizations that monitor water quality, and these can range from governments, private cottage associations, the academic community, or charities. A substantial concern with *in situ* collection methods is the financial cost and time investment required to complete and maintain a monitoring program (Lovett et al. 2007). This places considerable limitations on the number water resources that can be consistently monitored. The use of public and volunteer monitoring programs has been proposed to help alleviate the costs associated with a monitoring program while also increasing the area that can be sampled (Loperfido et al. 2010). With proper training, volunteer collection

of some variables is comparable to professionally trained employees (Obrecht et al. 1998). Public monitoring programs have taken place in Wisconsin (Rumery and Vennie 1988), Florida (Canfield Jr et al. 2002), and Nova Scotia, Canada (Sharpe and Conrad 2006) with considerable success. Unfortunately, volunteer programs require willing participants, which may be difficult to acquire for long-term studies or in remote locations.

Leave-in sampling options also exist for maintaining a long-term monitoring network. By placing sampling or monitoring equipment in water bodies of interest, a program can significantly reduce the personnel required to maintain a monitoring program. A sampling program in the Neuse Estuary in North Carolina used remotely accessible water quality sondes that measured many water quality variables (Springer et al. 2005). Leave-in sampling programs like this reduce costs associated with travel, and allow for targeted sampling during key events. Remote sensing also exists as a method for observing lakes, and advances in the capabilities of satellites, as well as reduced costs for use, have led to increased interest in using them for monitoring water bodies.

1.3 Remote Sensing

1.3.1 Non-satellite remote sensing

Remote sensing is the acquisition of data from an area without direct contact or physical data collection at the location. Aerial photograph analysis (photogrammetry) was one of the first methods of remote sensing and these methods are still in use today (Westaway et al. 2003). Modern remote sensing is often achieved with specialized sensors mounted on airplanes, boats, or orbital satellites. Light detection and ranging sensors (LIDAR - See Appendix A for glossary and abbreviations) can effectively survey and map areas by projecting a laser and

measuring the returning reflected light (Diaz et al. 2013). LIDAR is an active sensor, meaning is sends out a signal that interacts with an object and is then measured by the sensor. Spectrometers mounted on aircraft can also passively determine water quality based on the reflective properties of the variables of interest (Hakvoort et al. 2002). Passive sensors measure light reflected by objects, but requires light from another source such as the sun. Aircraft can be an excellent source of accurate remotely sensed data, but they can also have a very high operational cost (Mumby et al. 1998). These costs can quickly become prohibitive for monitoring a distant area or establishing a project that requires frequent data acquisition.

1.3.2 Satellite Remote Sensing

Early successes in oceanic water quality detection led researchers to use satellites designed for terrestrial applications for water quality monitoring. Many of the early water quality studies that utilized satellite imagery studied large water bodies, such as the Laurentian Great Lakes and the world's oceans (Kahru et al. 1994, O'Reilly et al. 1998, Stumpf et al. 2003). Large-scale water quality disturbances (such as large algal blooms) are easier to identify with the relatively coarse images produced by ocean color satellites like SeaWiFS and AVHRR. Both of these satellites have spatial resolutions of 1.1 kilometers. This limits these satellites, and ones of similar design, to larger water bodies. Near-shore areas and small inland water bodies could not be sampled because of the influence that the shoreline has on the light detected by a satellite.

The most notable group of satellites is likely the Landsat series, the first of which was launched on July 23, 1972 and the most recent launched on February 11, 2013. The Landsat series is longest continually running earth-observation satellite program. The program was

initiated by the National Aeronautics and Space Administration (NASA). Today however, the United States Geological Survey (USGS) has taken over distribution of imagery and management of the satellites. The Landsat satellites (mainly Landsat 5 and 7) have been used to monitor almost every water quality parameter that can be detected by a passive sensor since the program's inception. Some examples include Secchi depth (Kloiber et al. 2002), chlorophyll-*a* (Allan et al. 2011), phycocyanin (Kutser et al. 2006), and turbidity (Harrington et al. 1992). As of January 2009, all Landsat imagery was made freely available by the USGS (Woodcock et al. 2008). Before that time, images were approximately 600 dollars per image. Opening the Landsat archive caused an increase in the use of Landsat imagery by the public and scientific communities (Wulder et al. 2012). As such, the applications of the imagery have never been more widespread. More recent and advanced satellite platforms such as the QuickBird and IKONOS satellites have also been used for environmental monitoring purposes (Sawaya et al. 2003). These satellites have extremely high spatial resolution ($<1m^2$ pixels), and thus can identify very small spatial changes in both terrestrial and aquatic environments. However, this degree of accuracy does come with a high monetary cost. Newly acquired data from these satellites can cost about 20 dollars per square kilometer. Thus, imagery from multiple dates or over large geographic areas can quickly become too expensive to be a feasible option for most studies.

1.4 *Satellite Selection and Sensor Descriptions*

There are many satellites capable of aquatic monitoring. The appropriate satellite for a study depends greatly on the area and phenomenon of interest (Andréfouët et al. 2002). Cost-efficiency, temporal resolution, spectral resolution, and spatial resolution are four important

factors that are considered when choosing an appropriate satellite platform (Crétaux et al 2011). I chose to use the Landsat series of satellites because of their low cost, history of success, and their good balance between temporal, spectral, and spatial resolution.

The Landsat 4 and 5 satellites both contain the Thematic Mapper (TM) sensor, while Landsat 7 utilizes a more advanced version, the Enhanced Thematic Mapper (ETM+). Both the TM and ETM+ sensors use several bands (TM has 7, ETM+ has 8) that record reflected light from different wavelengths of the light spectrum. Bands 1 through 4 are of primary interest because they detect light in the visible and near infrared spectrum. The remaining bands are not useful for assessing the water quality variables I am interested in and were omitted (Bilge et al. 2003). Both the TM and ETM+ sensors are 8-bit (values range from 0-255) whisk broom sensors, which means they obtain an image one pixel at a time along the satellite's ground path. Landsat 7 imagery has suffered from a scan-line corrector failure since 2003 that has caused lines of data loss. However, the data between the lines remains useful and of high quality (Markham et al. 2004). Both sensors have a 30m spatial resolution, and operate on a 16-day revisit cycle. Landsat 5 and 7 are temporally spaced eight days apart making their combined temporal resolution approximately 8 days. It is relatively simple to translate data between the two sensors because they are very similar. This allows for analysis of a data archive that extends back to 1984 even though the images are taken from different Landsat satellites. In late 2011, the Landsat 5 satellite stopped functioning and image collection was suspended. As such, no Landsat 5 images were available for 2012. This reduced the effective revisit cycle to 16 days. The spectral and temporal properties of the Landsat satellites that were used in this study are presented in Table 1.1 below.

Table 1.1. Landsat 5 and 7 sensor properties. Bandwidth is similar between the satellites with a slight difference in band 4. The other bands are not included because they were not used in this study. Both satellites had the same 16 day temporal resolution.

Band Number	L5 Bandwidth (nm)	L7 Bandwidth (nm)	Spatial Resolution (m)
1	450-520	450-520	30
2	520-600	520-600	30
3	630-690	630-690	30
4	760-900	770-900	30

1.5 *Study Site Introduction*

Lake Diefenbaker (LD) is a large freshwater reservoir located in southern Saskatchewan, Canada (51^{o}1'53"N, 106^{o}50'9"W). The reservoir began to fill in 1967 when the construction was completed on two large earthen dams on the reservoir. The Gardiner Dam is located at the northern end of the reservoir and regulates flow of water into the South Saskatchewan River (SSR). This dam also has a hydroelectric power station that provides the region with electricity. The Qu'Appelle dam is located at the southern end of the lake, and regulates flow into the Qu'Appelle River (Fig. 1.1). The main source of water for the reservoir is the SSR, with 98% of the water in LD originating from this river (SWSA report, 2012). The SSR is fed by the Bow, Old Man, and Red Deer Rivers, which in turn draw the majority of their waters from snow and glacial melt in the Rocky Mountains. Inflow into LD from smaller creeks, rainfall, and runoff also contributes to the water levels in the reservoir, but these sources are minor in terms of water volume. The gross drainage area of the reservoir is over 140,000 km^2, and the majority of this area is agricultural land (SWSA report, 2012). The reservoir is approximately 225 km long and

has a surface area greater than 430 km^2. The reservoir has a maximum volume of 9.4 km^3 at the full supply level.

Fig. 1.1. Lake Diefenbaker and areas of interest. Water flows into the reservoir from the southwest and drains out of the Gardiner and Qu'Appelle dams. These dams are located at the ends of the Gardiner and Qu'Appelle arm. Additional labels represent towns, parks, and facilities located on or near the reservoir. Note that farm or ranch land surrounds nearly the entirety of the reservoir.

Water levels in the reservoir are managed primarily through the Gardiner Dam and vary significantly throughout the year (Bogard et al. 2012). The reservoir level can fall by as much as seven meters in the winter when inflows are typically lowest. These fluctuations can have a considerable effect on the ecology and physical structure of the reservoir (Thornton et al. 1990).

Lake Diefenbaker is a multipurpose reservoir, providing drinking water for over 45% of Saskatchewan's population. The South Saskatchewan River basin provides water for over 3 million people in Alberta, Saskatchewan and Manitoba. The reservoir is used for irrigation of

cropland, water for livestock, and recreational activities. A large fish farm located in a bay on the reservoir produces up to 1500 tonnes of fish yearly. The lake is also important for many local wildlife species. The endangered piping plover (*Charadrius melodus*) uses the beaches for nesting grounds, with up to 5% of the world's piping plover population nesting on the lake (Espie et al. 1998). Birds also use the lake to breed and as a feeding and resting site during migration. Approximately 26 native and non-native fish species can be found within LD. One of the most iconic fish that can be found in the lake is the lake sturgeon (*Acipenser fulvescens*), a protected species in the province (Pollock et al., submited manuscript; McLeod et al. 1999). Relatively little research has taken place that studies the water quality of the reservoir, despite its importance to the province and surrounding environment. Therefore, as development of LD and its watershed progresses, it is now vital to better characterize the reservoir's limnology.

1.6 Study Question and Rationale

A comprehensive study was started in 2011 with the goal of better understanding LD's water quality and limnology. Although there have been a few earlier research efforts that have examined LD (Hecker et al. 2012 and Patoine et al. 2006), this study is more comprehensive in size and scope. This research project is funded by the Global Institute for Water Security (GIWS) and covers a wide variety of research topics from nutrient loading, mass balance, algal composition, fish study, and more. My own study complements these studies by providing a synoptic view of the entire reservoir using Landsat imagery and extracting water quality information from it. Some residents living near the lake have suggested that increased algal activity has been taking place in recent years, and this study will be able to investigate these claims with archived satellite imagery.

The primary research goal of this study is to use the Landsat series of satellites to predict the water quality variables chlorophyll-*a* (Chl-*a*) and Secchi disk depth (SDD) at Lake Diefenbaker. A significant assumption of this monitoring method is that changes in the water quality variables mentioned above are detectable by the Landsat satellites. Increases in Chl-*a* concentration should cause an increase in satellite-detected reflectance as more light is reflected by the algae in the water. Increases in reflected light should also be a sign of reduced SDD, as turbidity, sediment, and algae will cause a reduction in water clarity. Conversely, clear waters should reflect smaller amounts of light, resulting in deeper SDD's. The Landsat data archive will also be useful in obtaining water quality information dating back to 1984. I had a number of objectives that would help accomplish the primary goal of this research, which are presented below.

1.7 *Study Objectives*

1. Using Landsat satellite imagery, develop a predictive model using the relationship between satellite derived reflectance and water quality variables (Chl-*a* and SDD) at LD during 2011 and 2012 and apply the models to imagery from these years.
2. Assess the accuracy of these newly generated models, and determine how a time-lag affects their explanatory power.
3. Apply the models to a large data archive of Landsat imagery that dates from 1984-2012
4. Using the data generated from these models, investigate the magnitude and some potential causes of long-term trends in Lake Diefenbaker water quality.
5. Determine how ephemeral events such as algal blooms and high flow events affect Lake Diefenbaker's water quality.

Chapter 2 - Modeling Chlorophyll-*a* and Secchi Disk Depth Using Landsat Satellites in a Large Prairie Reservoir [1]

2.1 Introduction

Water quality monitoring is an important component in the maintenance of healthy aquatic ecosystems. The stakeholders and managers of these aquatic systems need timely and complete data to properly manage these systems. Chlorophyll-*a* concentration and Secchi disk depth have been consistently used to monitor and measure water quality and the trophic status of lakes. These variables are relatively easy to collect and are useful for assessing aquatic health (Carlson 1977). Chlorophyll-*a* concentration (Chl-*a*) can be used as an approximation of the algal biomass in the water and Secchi disk depth (SDD) is related to water clarity and turbidity. The Secchi disk is a conventional and relatively simple instrument. It is still a useful tool because measurements are easy to collect and other water quality parameters can be easily and accurately derived from Secchi Disk values (Boyce et al. 2010). Chlorophyll-*a* concentration tends to positively correlate with increased nutrient loading to water bodies (Schindler 1974), and thus is a good estimate of eutrophication. Eutrophication can lead to algal blooms of increased size, duration, and magnitude in many aquatic systems. Therefore, the detection and management of algal biomass and water quality in water bodies is very important. Traditional methods of water quality monitoring that can detect changes in water quality can be time-consuming and costly (Lovett et al. 2007; Nelson et al. 2003). As a result of the potentially high costs, water quality monitoring requires an inexpensive alternative that can deliver useful and high quality data.

[1] **Note** This chapter of my thesis is written in a manuscript style. As such, there will be some overlap between this chapter and other chapters of the thesis.

Remote sensing has become a feasible alternative or supplement to *in situ* monitoring because the cost of imagery has decreased in recent decades. The use of remotely sensed data has been shown to effectively predict several water quality variables in lakes, bays, estuaries, reservoirs, and oceans. These variables include chlorophyll-*a* concentration (Torbick et al. 2008), Secchi disk depth (Olmanson et al. 2008), turbidity (Harrington et al. 1992), surface water temperature (Giardino et al. 2001), and more. There are many satellites that have been used in these studies, but the Landsat series of satellites has been particularly valuable in this field for over 30 years. They are effective because they have a good compromise between temporal, spatial, and spectral resolution. Furthermore, imagery is now readily accessible and is archived back for several decades. While Landsat has been used to accurately characterize lakes, fewer studies have examined their lakes of interest over a long period of time. Instead many studies focus on one (Brezonik et al. 2005; Nas et al. 2010) or a few images (Duan et al. 2008). Some studies on the other hand investigate many images, but generate models for each image using corresponding field data. These methods are excellent when used as a supplement for field sampling, but these methods restrict the studies from extracting archived data without corresponding field data. As a result, images without this field data cannot be used to extract water quality data, and hindcasting from past imagery would be difficult.

LD is a large reservoir located in southern Saskatchewan. The reservoir is important economically, recreationally, and also provides drinking water for a large portion of the province's population. The reservoir began to fill once the construction of two large earthen dams was completed in 1967. These two dams, the Qu'Appelle and Gardiner dams, regulate flow into the Qu'Appelle and South Saskatchewan Rivers (SSR) respectively. A large

hydroelectric power station is also integrated into the Gardiner dam. The reservoir and surrounding area is home to many species of fish and animals and is an important rest-stop for thousands of migratory birds each year. Despite the reservoir's importance to the province, its limnology and associated water quality have been understudied since its completion. This study, as a part of a larger Global Institute for Water Security (GIWS) research program aims to better characterize the limnology and water quality of the largest water body in southern Saskatchewan.

This study used the Landsat 5 Thematic Mapper (TM) and Landsat 7 Enhanced Thematic Mapper (ETM+) sensors to quantify the chlorophyll-*a* and Secchi disk depth at LD during May-October of 2011 and 2012. These satellites were chosen because of their low cost and spectral resolution that is capable of identifying changes in the water quality variables of interest. This study had a number of objectives: First, I wanted to develop models that could predict water quality variables (SDD and Chl-*a* concentration). These models can complement or reduce the need for future field sampling. This in turn could provide more complete data, or reduce future study costs. A second objective I had was to assess the effect of a time lag between image acquisition and field data sampling. Many studies assume this effect is negligible, but I wanted to confirm if there is a significant effect on satellite models at Lake Diefenbaker. As a third objective, I wanted to compare the predicted water quality variables to actual data taken at the same time that was not used in model development. This objective would allow me to comment on the model's effectiveness. Fourth and finally, I wanted to assess trends in both SDD and Chl-a concentration at the reservoir using predicted data and imagery. In addition, I also wanted to investigate a few potential events that may contribute to any trends in water

quality at LD. As such, I investigated the effect of flow, and the effect of algal blooms on SDD and Chl-*a* concentration. Analyzing the trends in LD will allow reservoir managers to better predict future water quality changes in the reservoir.

2.2 Methods

2.2.1 Field Collection Methods

It was first necessary to gather field data in order to develop models for predicting water quality. Data that was used in model generation was collected during 2011 and 2012. Field data collection occurred on the same day as satellite image acquisition when possible. Satellite image acquisition took place at approximately 10:30 local time, and sampling took place within four hours of this time. For 2011, sampling took place from early August to the end of October. In 2012 the field season was extended from June to October. In both years, sampling took place every eight days. In 2011, both Landsat 5 and 7 were operational, so each eight day cycle alternated between the two satellites. In 2012, Landsat 5 became non-operational. However, the fortuitous location of the reservoir in relation to the satellite paths, Landsat 7 was still able to image a majority of the reservoir every eight days.

Field sampling took place at a total of 16 field sites in 2011, and 24 in 2012 (Fig. 2.1) Field sites were chosen in areas with water sufficiently deep to eliminate any influence of the reservoir bed on satellite reflectance. They were also selected far enough from the shore to eliminate any error caused by water-land interface pixels. Two replicated water samples were collected from a depth of 1m using a Van Dorn sampler. I assumed the mixing depth of the reservoir would always exceed several meters, and therefore deemed a discrete sample from a depth of 1m would be representative of surface waters. These assumptions eliminated the

need for an integrated water sample. The water samples were stored in opaque 2-litre bottles and placed in coolers to prevent Chl-*a* degradation. Upon return to the laboratory, the samples were refrigerated. SDD measurements using a 20cm diameter freshwater disk were taken on the shaded side of the boat to ensure consistency. A Yellow Springs Instruments (YSI) water quality sonde was deployed at a number of sites to acquire additional water quality information including phycocyanin fluorescence, turbidity, temperature, and other variables. Additional Chl-*a* samples and SDD measurements were also taken by a concurrent GIWS study. Flow rates into LD were obtained by Environment Canada water quality stations (http://www.wsc.ec.gc.ca/applications/H2O/index-eng.cfm).

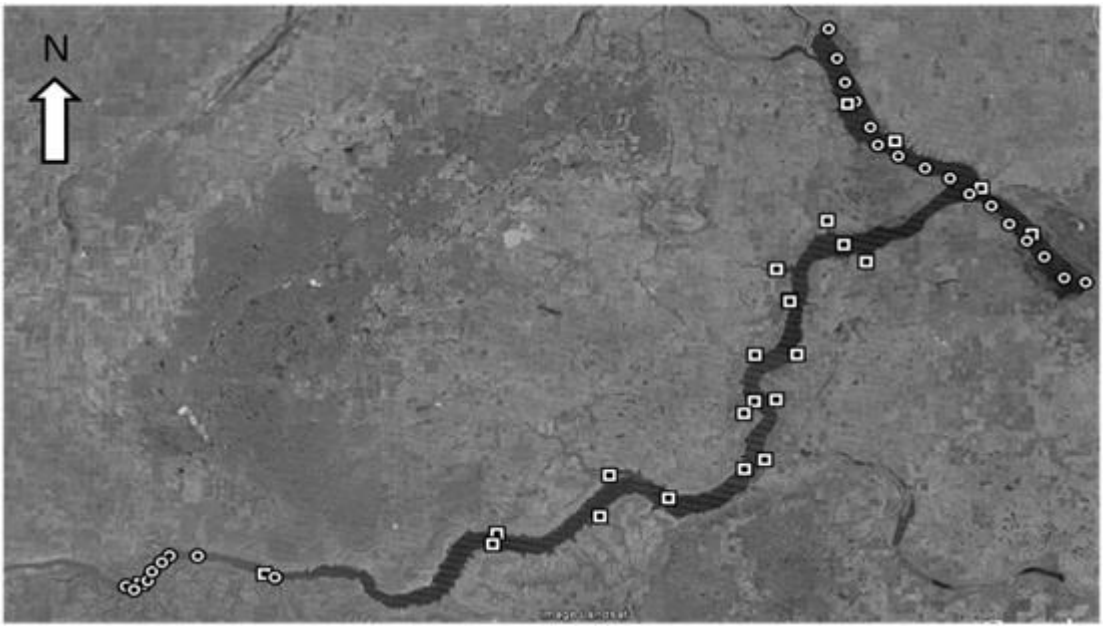

Fig. 2.1. Lake Diefenbaker sampling locations. These points illustrate where SDD and Chl-*a* data was acquired. This data was used to calibrate and develop models for the satellite imagery. Circular sites were sampled on the same day as the Landsat images were taken, while square sites were used where applicable. These square sites were part of the concurrent study that took place on LD.

2.2.2 Laboratory Processing

Water samples were processed for Chl-*a* within 24 hours using the process described by (Bergmann and Peters 1980). In brief, water samples were filtered through a 47mm glass fiber filter with a nominal pore size of 0.8 microns. Filters were then frozen until extraction for Chl-*a*. Filters were then cut into strips, and bathed in ethanol for approximately 24 hours to extract Chl-*a.* Reflectance was then measured on a spectrophotometer at 750nm, 650nm, and 649nm to determine Chl-*a* concentration from the solution. Both samples of reservoir water were filtered and extracted. The data was then averaged from these two replicates.

2.2.3 Image Processing

All satellite imagery was obtained from the USGS through the Global Visualization Viewer website (glovis.usgs.gov). Lake Diefenbaker lies along paths 37 and 38, and rows 24 and 25 of the WRS-2 orbit. Satellite imagery was downloaded and converted into a useable format in PCI Geomatica (Version 10.3). Two images from the same path, but different rows from each sampling day were combined into a single image for analysis because the reservoir's size exceeds a single image. On Path 38, a small section of the Qu'Appelle arm of the reservoir was not visible. Images were then processed using PCI Geomatica software (Version 10.3.1). Landsat bands 1-4 were combined into a single image. Images were then clipped to a smaller size to include only LD and the immediate area to reduce processing times. Clipped and combined satellite images were then atmospherically and radiometrically corrected. Atmospheric correction was accomplished using an improved dark-object subtraction method described by (Chavez 1988). A homogenous horizontal atmosphere was assumed when performing the correction. Radiometric correction required the use of satellite specific

exoatmospheric irradiance correction, gain, and bias data which was acquired from Chander et al. (2009). Image data was translated from a raw brightness value to a radiance value for each band ($W \cdot ster^{-1} \cdot m^{-2}$, Equation 2.1). In this equation, L^{λ}= Spectral Radiance at Sensor Aperture ($W/(m^2\ ster, \mu m)$], DN = Raw Digital Number (Integer value 0-255), DOS = Dark Object Subtraction Calculated Value (Integer Value), Gain = Band Specific Rescaling Gain Factor ($W/(m^2\ sr, \mu m)$], and Bias = Band Specific Rescaling Bias Factor ($W/(m^2\ sr, \mu m)$].

Equation 2.1: $L^{\lambda} = Gain \times (DN*DOS) + Bias$

Radiance was converted into a unitless reflectance value (Equation 2.2). In this equation, P_p = Reflectance Value, π= Mathematical constant equal to ~3.14159 (unitless), $L\lambda$ = Spectral radiance at the sensor's aperture [$W/(m^2\ sr\ \mu m)$], d =Earth-Sun distance (AU), $ESUN_{\lambda}$ = Mean exoatmospheric solar irradiance[$W/(m^2\ \mu m)$], and θs= Solar zenith angle (degrees)

Equation 2.2: $$\rho_P = \frac{\pi * L_{\lambda} * d^2}{ESUN_{\lambda} \cos\theta_s}$$

Raw satellite values were converted to reflectance values because it allows for comparison of results across multiple dates and images. This allowed for a single model per variable for the instead of one model for each day. Reflectance data from bands 1-4 was then extracted from the images at the same coordinates where the field samples were taken. A 3 x 3 pixel filter averaged the area surrounding the sampled location to reduce the effect of erroneous or outlier pixels. Sections of images that had cloud cover or haze were not used in the analysis, as these phenomena had a significant and unpredictable effect on reflectance values. The malfunction SLC onboard Landsat 7 caused repeating lines of data loss on all

images taken after 2003. Data that is not within these lines is unaffected. The stable orbit of the satellite ensured that field sampling rarely took place within the missing data areas of the ETM+ imagery. If the missing data lines occurred over a field site it was excluded or moved. If a useful data pixel was within 300 meters (10 pixels) of the missing field site, then it was assumed that the reflectance value in that pixel was representative of the missing data and included in analysis. If it was farther than 300 meters, that data was excluded from analysis.

2.2.4 Statistical Analysis and Model Application

The R statistical environment (Version 2.15.2) was used for all statistical analyses. Figures were generated in R, PCI Geomatica, and Microsoft Excel. The normality of water quality variables was assessed using the Shapiro-Wilk test, and an examination of a Quantile-Quantile (QQ) plot. The relationship between SDD and Chl-*a* concentration was examined with regression analysis. A relationship was then developed between the satellite-derived reflectance and the water quality variables of interest (Chl-*a* and SDD). The SDD and Chl-*a* samples were treated as the response variables and band reflectance values were treated as the independent variables.

Regressions between water quality variables (SDD and Chl-*a* concentration) and single band, combinations of multiple bands, and band ratios were all used in an attempt to develop relationships and complete the first study objective. The best models for each variable were found by using multiple linear regressions, and then eliminating bands that didn't significantly contribute to the predictive models using the Akaike Information Criterion (AIC). This was repeated until there was a loss in model significance. I determined that the best model would be the one with band combinations that had the highest R^2 value. After the best models were

identified, a second statistical analysis was used to assess the effect of a sampling time lag and fulfill the second objective of this study. The number of days separating the field data collection date from the satellite image acquisition date was recorded during field acquisition. The regression models were initially developed so that they only had data that had been acquired on the same day as image acquisition. To test the effect of sampling lag, data that had a single day of separation was also included and the models were tested again. After this step, data from two days or fewer were added and the regression models were analyzed again. This continued until a five day time lag was included in the SDD model, and a three day model was included in the Chl-*a* model.

To satisfy the third study objective of this study, data obtained by the concurrent GIWS study in 2011 and 2012 was used to compare predicted Chl-*a* concentration and SDD to field sampled data was used to assess the accuracy of the models. Data from field sites was extracted from modeled images and compared to field data from the same locations. Regression models and root-mean-squared-error (RMSE) were used to assess model accuracy. The accuracy assessment used field data that was not collected on the same day as image acquisition, so time-lagged models were used for this assessment. Data used in the assessment was collected in both the 2011 and 2012 field seasons. To prevent a modeling bias, field data used to generate models was not used in the model accuracy assessment.

The models that included the most data and explained the highest R^2 were then selected to model the entire reservoir and complete the fourth objective of this study. The regression coefficients from the SDD and Chl-*a* models were processed in PCI Geomatica, and two new image channels with predicted Chl-*a* and SDD values were added to each satellite

image. Data was then extracted from the reservoir using these newly generated image channels. Instead of acquiring data from the entire reservoir, sixteen data points were extracted from the reservoir and used as to quantify yearly cycles of SDD and Chl-*a* in the reservoir (Fig. 2.2). This data was also used to investigate any algal blooms that were detected at LD. Color maps were produced to visualize reservoir trends.

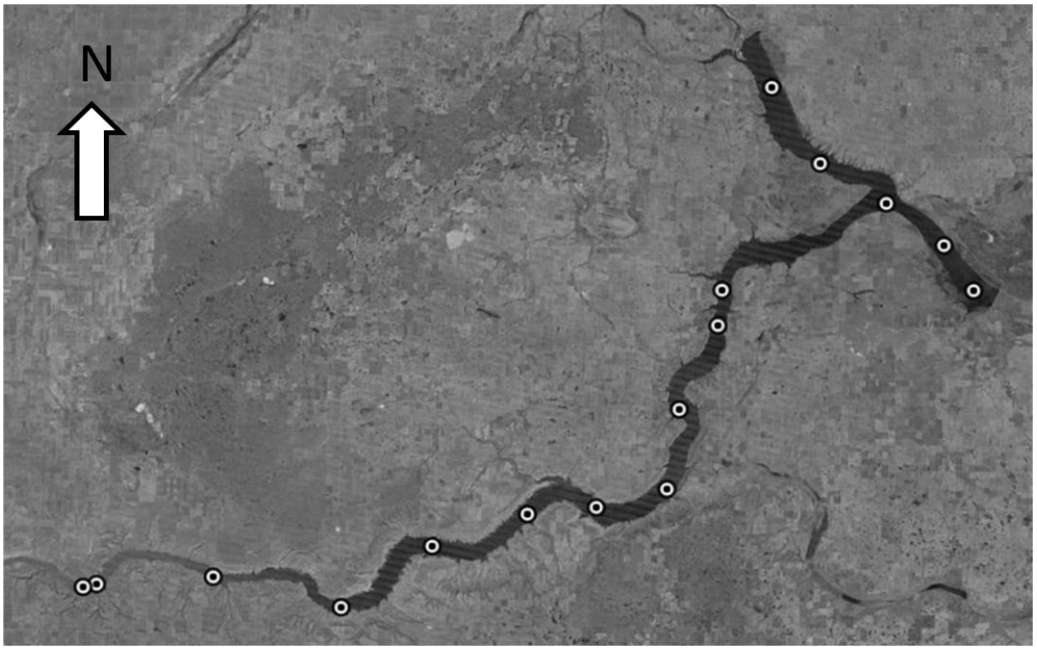

Fig. 2.2. The points on this figure represent areas where water quality data was predicted from Landsat imagery. All areas were separated from shore to ensure no reservoir bottom interference was present.

2.3 Results

2.3.1 Field Data Summary

A total of 20 sampling days were attempted throughout the 2011-2012 field seasons. A number of days were unsuccessful due to inclement weather, equipment failure, or cloud-covered imagery. As a result, water quality data from only 13 days were included in statistical analysis. Of those 13 days, some had partial cloud cover and therefore only the data points outside the cloud cover were used for analysis. Sampling days are summarized below (Table

2.1). Field data and images were acquired primarily on the same day, but a concurrent study was able to collect data on days between image acquisitions. The data from this adjacent study was included in the models when it fell within an acceptable time-window (within 3-5 days). The data was collected using the same sampling protocols as my data. Data used in the accuracy assessment also came from this adjacent study.

Table 2.1. Field sampling and imaging schedule results. The sampled column indicates whether field sampling occurred on this date or not. The imaged column indicates whether or not there was a useful image for model generation. The Used for modeling column indicates if the image data was used in model generation.

Date	Sampled?	Imaged?	Used for modeling?
August 24, 2011	Yes	Yes	**Yes**
September 1, 2011	Yes	Yes	**Yes**
September 9, 2011	Yes	Yes	**Yes**
September 17, 2011	No	No	No
September 25, 2011	Yes	Yes	**Yes**
October 3, 2011	Yes	No	No
October 12, 2011	Yes	Yes	**Yes**
October 19, 2011	Yes	No	No
June 23, 2012	Yes	Yes	**Yes**
June 30, 2012	Yes	Yes	**Yes**
July 9, 2012	Yes	Yes	**Yes**
August 1, 2012	Yes	Yes	**Yes**
August 10, 2012	Yes	Yes	**Yes**
August 17, 2012	Yes	No	**No**
August 26, 2012	No	No	No
September 5, 2012	Yes	Yes	**Yes**
September 18, 2012	No	No	No
September 26, 2012	Yes	Yes	**Yes**
October 5, 2012	No	No	No
October 13, 2012	No	No	No

Field collected samples at LD had a mean Chl-*a* concentration of 5.98 µg L^{-1} (range = 0.98-16.54 µg L^{-1}, 95% CI [0 µg L^{-1}, 17.84 µg L^{-1}]). A maximal chlorophyll reading during an ancillary sampling event measured over 1600 µg L^{-1}. This sample was not collected with the standard collection protocols mentioned above, and was excluded from analysis. Mean SDD was recorded as 3.24m (range = 0.1m-6.5m, 95% CI [0.66 m, 6.84 m]).

Data from Environment Canada flow stations measured inflowing water from the SSR (Fig. 2.3). Although some inflow entered the reservoir from Swift Current Creek, rainfall, and runoff, this amount was small enough to be considered negligible, and not included in the figure below.

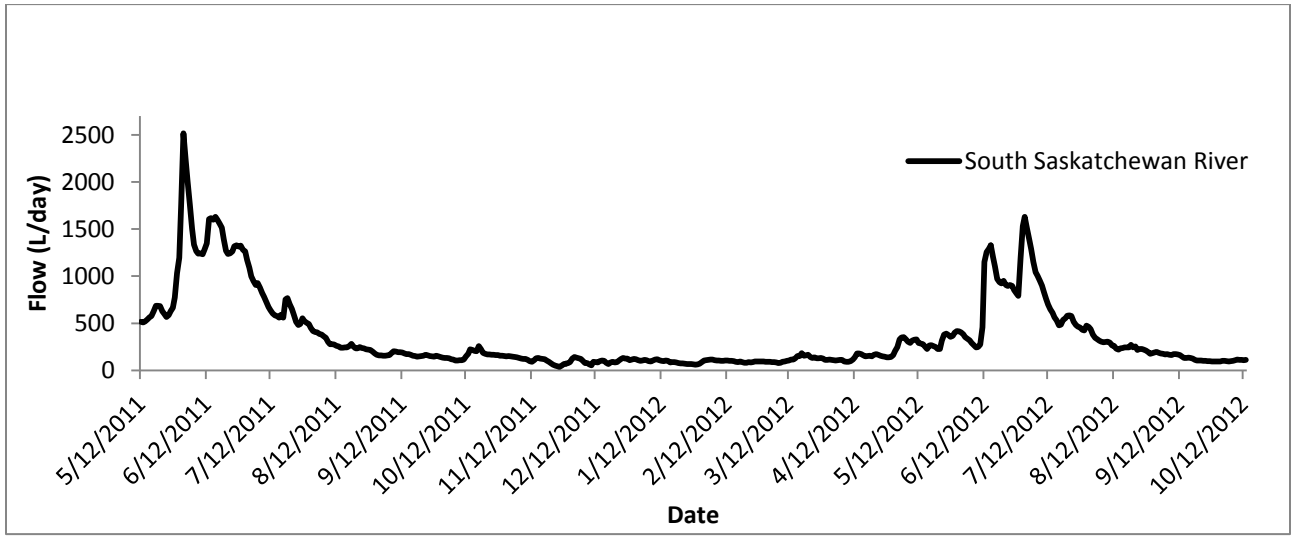

Fig. 2.3. Water flow into LD during the 2011 and 2012 seasons. The 2011 season had markedly higher flow than 2012, but both years are considered high flow years. Note the considerable spikes in flow rate that exist in May-July.

2.3.2 Image Processing Results

Over 50 Landsat 5 and 7 images were obtained and corrected for the 2011-2012 seasons. However, only 26 images could be used for developing models because of cloud interference. Image acquisition took place at approximately 10:30 local time. The majority (20)

of the images used were Landsat 7 ETM+ images, with the remainder (6) being Landsat 5 TM images. The termination of the Landsat 5 program in November 2011 meant that all imagery from 2012 was from the Landsat 7 satellite. Due to an error aboard the Landsat 7 satellite, all ETM+ had imagery affected by SLC failure (Fig. 2.7 shows SLC stripes).

2.3.3 Statistical Results

Chlorophyll-*a* concentrations and SDD data was normally distributed, and therefore it was not necessary to transform data for analysis. There were positive relationships between Chl-*a* concentration and SDD (predicted data; R^2=0.27, p-value<0.0001, and reference data; R^2=0.05, p-value=0.09, respectively). Single and multiple linear regressions between satellite-derived reflectance and Chl-*a*/SDD were derived to create models that predict water quality (Table 2.2). These regression values include a sampling lag of up to three days for Chl-*a* and five days for SDD.

Table 2.2. This table presents the single band regression (SR), band ratio regression (BR), and multiple regression results (MLR). N/S indicates a non-significant result (p-value<0.05), and numerical values are the R^2 values. The bolded terms indicate the band combinations that were used for predicting water quality variables.

Band/Combination	**n (Chl-*a*)**	**Chlorophyll-*a* R^2**	**P (Chl-a)**	**n (SDD)**	**Secchi Disk Depth R^2**	**P (SDD)**
Band 1 SR	79	N/S	N/A	118	.09	<0.001
Band 2 SR	79	N/S	N/A	118	.137	<0.001
Band 3 SR	79	.005	.048	118	.265	<0.001
Band 4 SR	79	.39	<0.001	118	.461	<0.001
1/2 Ratio BR	79	.11	.043	118	.246	<0.001
1/4 Ratio BR	79	.23	<0.001	118	.45	<0.001
2/4 Ratio BR	79	.36	<0.001	118	.148	<0.001
3/4 Ratio BR	79	.42	<0.001	118	.420	<0.001

4+2+1 MLR	79	.39	<0.001	118	**.55**	<0.001
4+3 MLR	79	**.45**	<0.001	118	0.48	<0.001

For SDD, the strongest relationship was found using bands 4, 2, and 1(Fig. 2.4, panel 1). For Chl-*a*, the strongest relationship was found using Bands 4 and 3 (Fig. 2.4, panel 2). These models were used for time lag analysis and accuracy assessment.

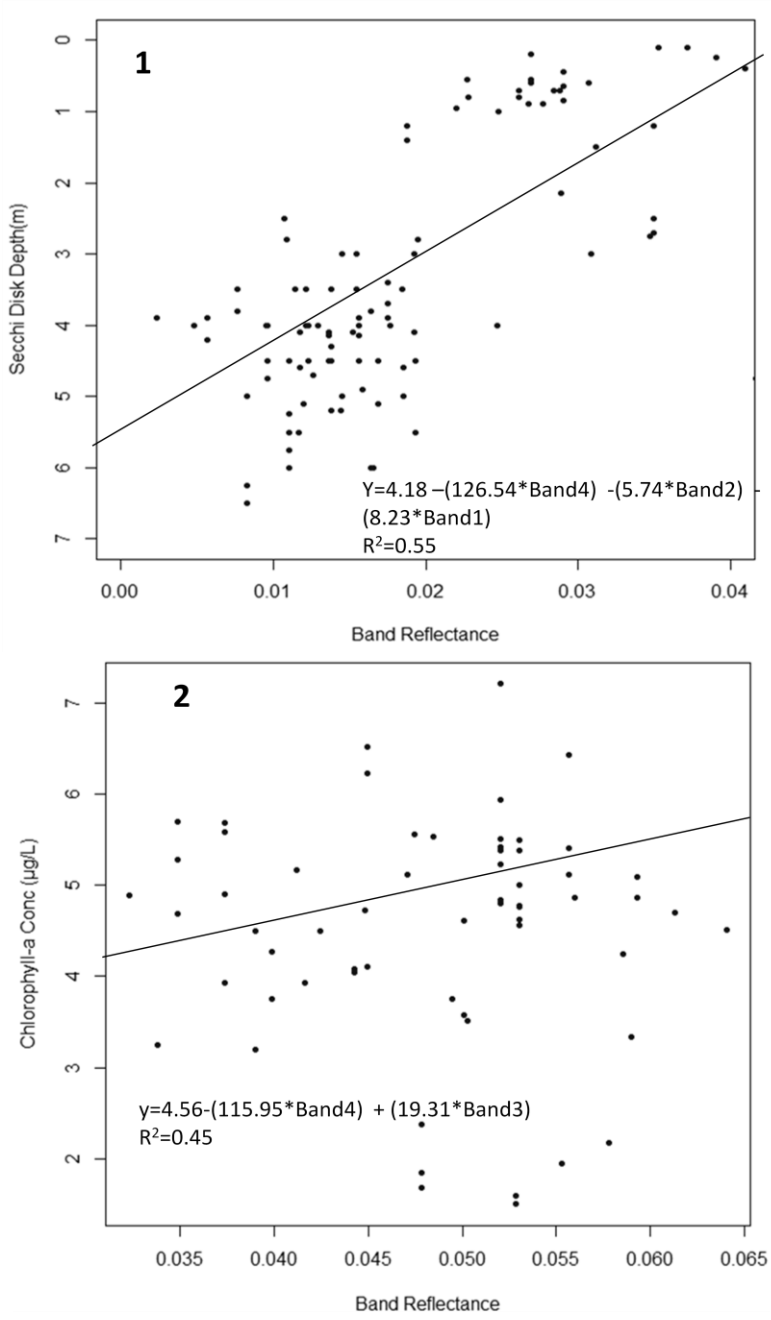

Fig. 2.4. The regression models that compare band reflectance and water quality. Regression equations are presented in the bottom segments of the graphs along with the associated R^2 values. Note that in panel 1, the y-axis is reversed.

2.3.4 Time Lag Analysis Results

The effect of increasing separation dates between sampling and satellite measurement were assessed on SDD readings and Chl-a (Table 2.3).

Table 2.3. The effect of separation date on the models used to predict SDD and Chl-*a*. The SDD models show in model strength as the time-lag increases. The Chl-*a* model strength remained similar as the time-lag increases.

Days of Separation	Secchi Disk Depth R^2	Chlorophyll-*a* Conc. R^2
0	0.69	0.40
1	0.61	0.40
2	0.58	0.42
3	0.53	0.45
4	0.52	No Supplemental Data
5	0.55	No Supplemental Data

The strength of the SDD relationship decreased as the time lag between sampling date and imaging date increased. The greatest changes in the SDD relationship strength occur after the first two days of the time lag are introduced. For Chl-a concentration, there was no reduction in model strength when including data from up to three days between sampling and imaging. The models that included the greatest time window (five days for SDD and three days for Chl-*a* concentration) were used to predict further water quality data.

2.3.5 Model Accuracy Assessment Results

An assessment of model accuracy showed that both models have a positive relationship between predicted and actual Chl-*a* (R^2=0.62, p=0.0014, n=42) and SDD values (R^2=0.56, p<0.0001, n=42). For SDD, there was no predictive bias, and error was relatively evenly distributed (Fig. 2.5; Panel 1). The RMSE for the SDD model was 1.01 m.

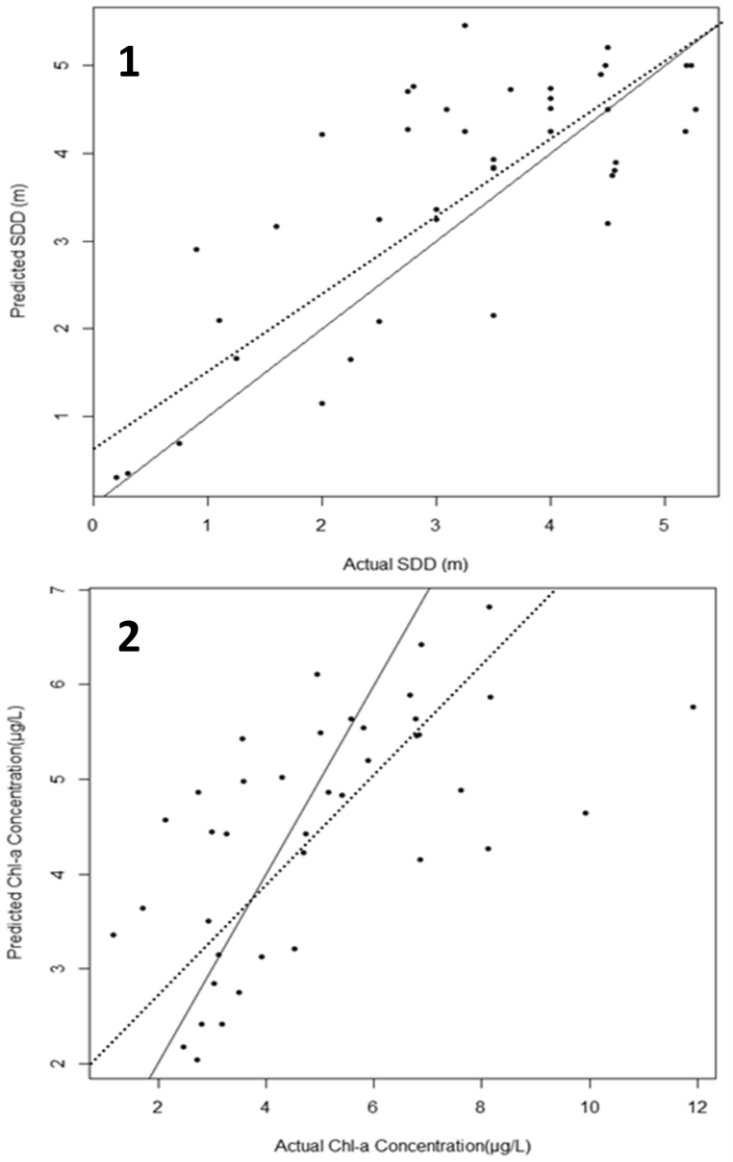

Fig. 2.5: Predicted data compared to actual data for SDD (panel 1) and Chl-*a* concentration (panel 2). A 1:1 slope line (solid line), and a linear regression model (dashed line) shows the relationship between predicted and actual data. Data used in this analysis was independent, and not used for model development.

The Chl-*a* model was shown to be less effective at predicting high chlorophyll-*a* concentrations. The bias was an underestimate; field-reference Chl-*a* tended to be higher than my predicted estimate. In addition, the higher RMSE of 2.54 µg L^{-1} indicated that the Chl-*a* model is less effective at predicting actual values when compared to the SDD model. The

model can still predict changes in Chl-*a* concentration, and it can also detect the presence and extent of algal blooms (Fig. 2.6). As such, I determined that it would be acceptable for modeling LD.

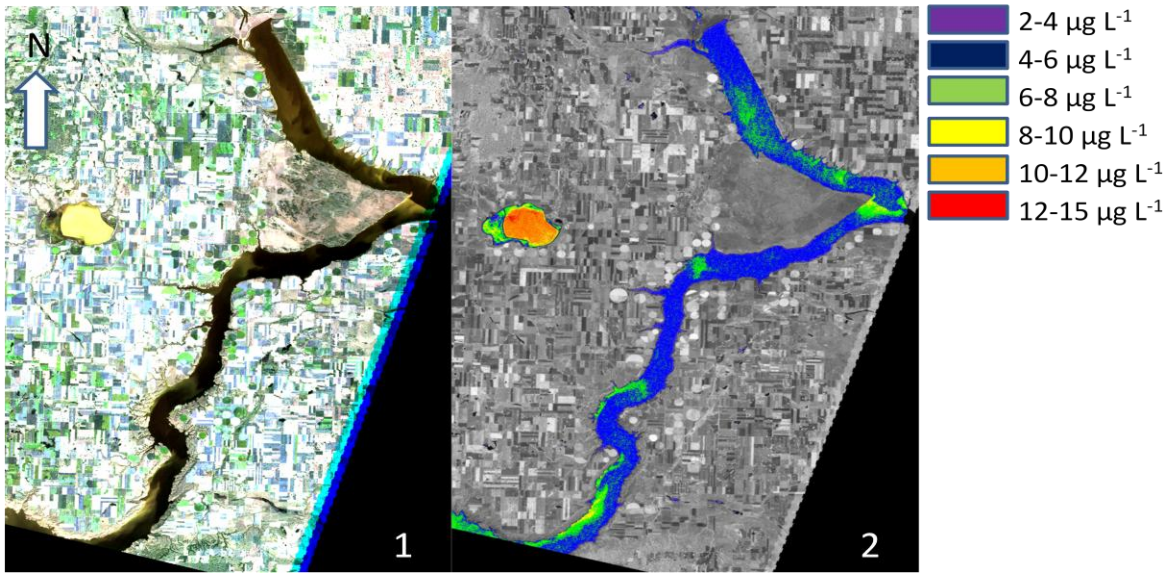

Fig. 2.6. Algal blooms imaged by a true color satellite image (panel 1) and modeled image (panel 2). Blooms are characterized by green water that represents an algal scum. The smaller body of water west of LD is Lucky Lake, an area that typically has a high algal biomass. This image was acquired on August 29th, 1999.

I determined that the predictive SDD model which included data from up to five separation days should be used for modeling the reservoir, despite its slightly lower explanatory power. This greater amount of data suggests that this model is more robust because it includes a wider variety of reservoir conditions. I also decided that since the Chl-*a* concentration model did not lose explanatory power when a greater number of separation days were included, it was useful to use the model that incorporated up to three separation days as well.

2.3.6 Model Results

At LD, it was possible to obtain an image of the reservoir every 8 days. However, cloud cover made it impossible to achieve a consistent temporal resolution that was finer than one image per month. Mid-month images were used where months had more than one available image. The mean Chl-*a* concentration predicted by the models during 2011 and 2012 was 5.64 $\mu g\ L^{-1}$ (Range = 1.41 $\mu g\ L^{1}$-9.82 $\mu g\ L^{-1}$, 95% CI [0.67 $\mu g\ L^{-1}$, 10.56 $\mu g\ L^{-1}$]) in the predicted field sites, similar to the field data mean of 5.98 $\mu g\ L^{-1}$. The mean SDD predicted by the models was 3.4 m (Range 0.1 m-5.98 m, 95% CI [0.70 m, 6.68 m]), again similar to the field data mean of 3.24m. Modeled images were converted into color maps to illustrate spatial and temporal changes in Chl-*a* concentration and SDD in the reservoir. The color maps are coded so that a range of depths and concentrations are presented with a unique color for each range for SDD (Figs. 2.7-2.9) and Chl-*a* (Figs. 2.10-2.12) respectively. Only 2012 maps are presented, but the patterns observed in 2011 are similar in 2012. The changes in each variable are presented by a series of three images. Imagery shows a notable reduction in water clarity in June (Fig. 2.8), but this reduction is absent in May (Fig. 2.7) or September (Fig. 2.9). This reduction in water clarity is greatest near the SSR inflow, and reduces in intensity in the downstream portions of the reservoir. Algal concentrations are highest in the downstream portions of the reservoir in May, and lowest near the SSR inflow (Fig. 2.10). The same pattern is observed in September (Fig. 2.12), but algal concentrations are generally higher at this time. In June the pattern is opposite, with higher concentrations in the upstream portions of the reservoir and lower concentrations in the downstream portions (Fig. 2.11).

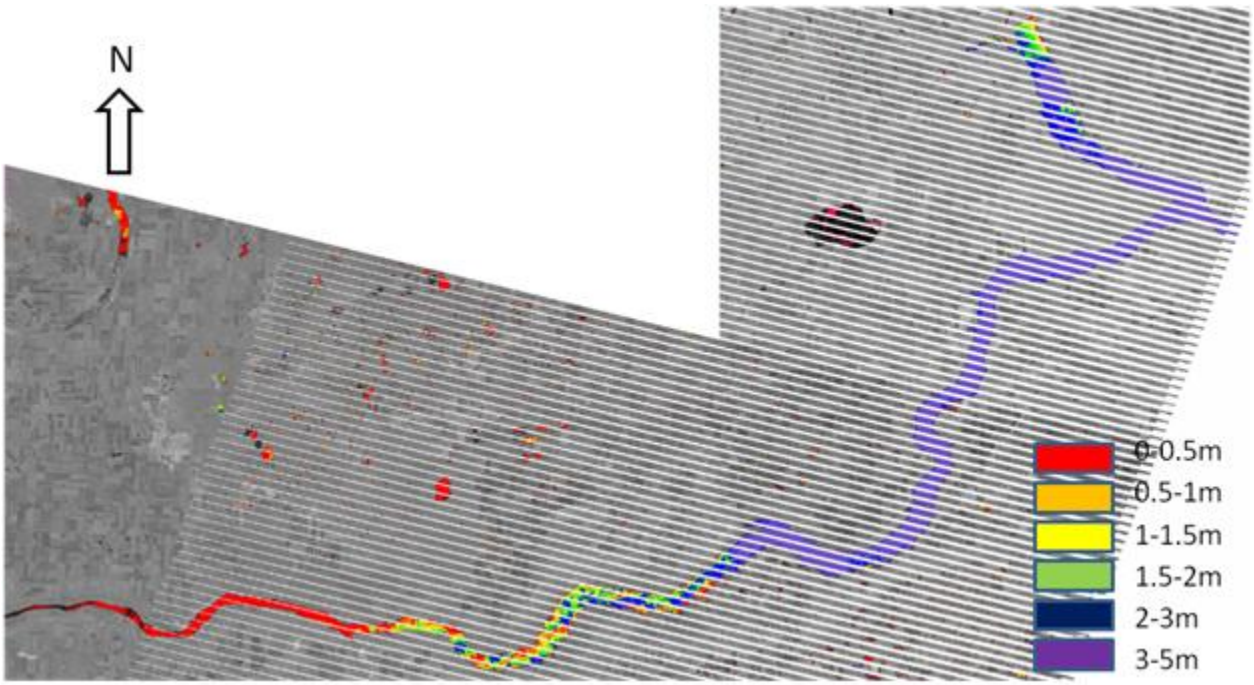

Fig. 2.7. May 29th, 2012 Secchi disk depth. This image shows the early progression of a sediment plume arriving from the mountains near the SSR inflow at the southwest end of the reservoir. SDD in the central and eastern sections of the reservoir are deeper. The legend on the bottom right illustrates the range in SDD. Colored areas represent water, while grey areas are land. The white lines are caused by an SLC error on the ETM+ sensor.

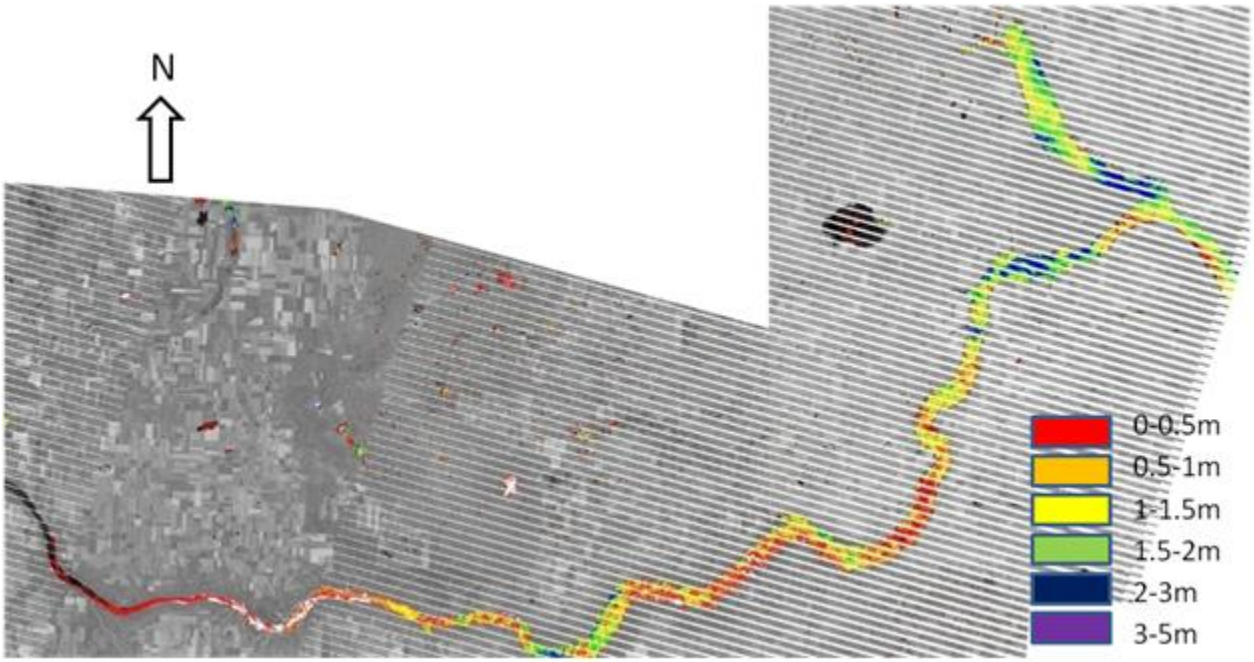

Fig. 2.8. June 29th, 2012 Secchi disk depth. This colored image shows the near-maximal progression of the sediment plume that arrives from the SSR. SDD is relatively shallow throughout the entire reservoir. A small section of the Qu'Appelle arm (eastern corner) is not imaged due to the angle in satellite path. Colored areas are water and grey areas are land.

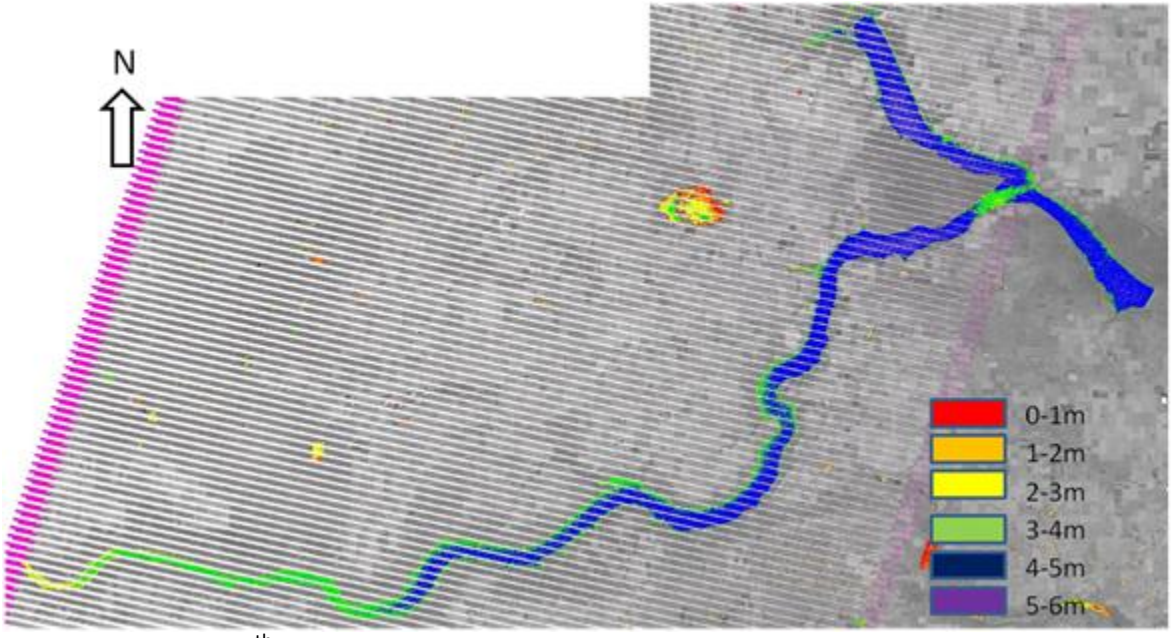

Fig. 2.9. September 27th, 2012 Secchi disk depth. This figure shows that the sediment plume is no longer detectable in the majority of the reservoir. The western portion of the reservoir where the SSR enters has notably shallower SDD's. Note that the legend is different from the previous two figures.

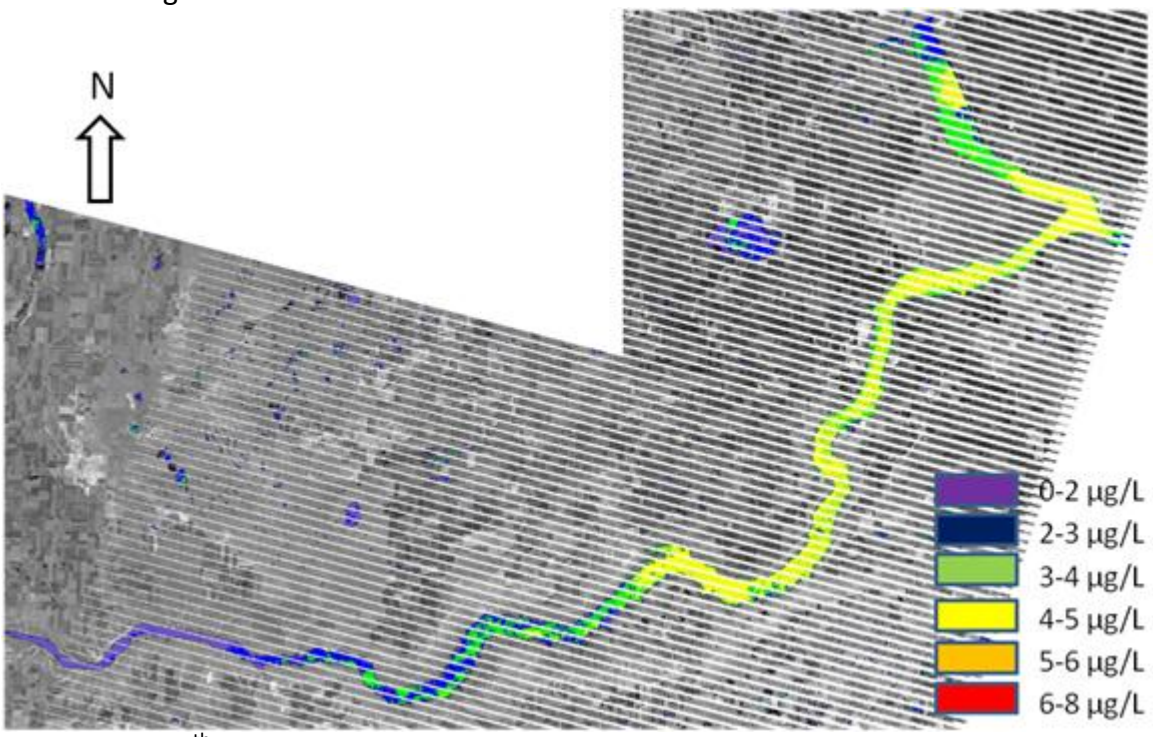

Fig. 2.10. May 29th, 2012 chlorophyll-*a* concentration. This map shows that after the ice comes off, Chl-*a* is highest in the downstream portions of the reservoir, and lowest near the inflow. Blooms are absent, and the sediment plume it has not reached the majority of the reservoir. Colored areas represent water, while the areas colored grey represent land.

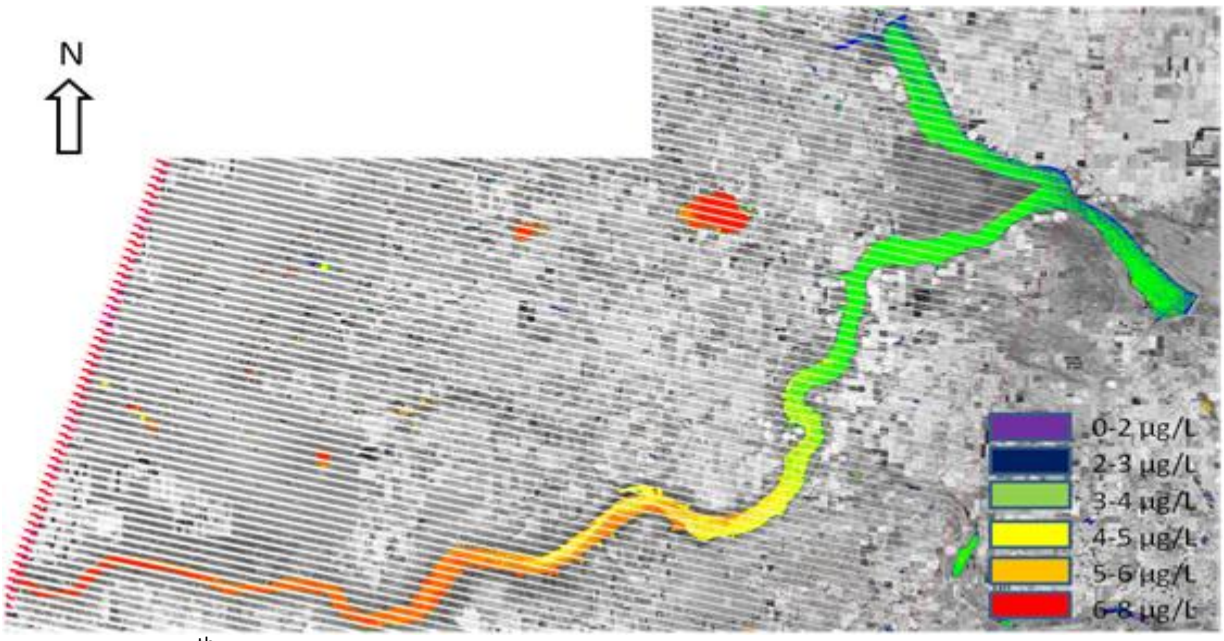

Fig. 2.11. July 9th, 2012 chlorophyll-*a* concentration. Chl-*a* concentration is greater in the western portion of the reservoir than in the eastern 'arms' of the reservoir. The pattern follows the behavior of the sediment plume, with higher chl-*a* concentrations inside the plume than outside. Colored areas represent water, while the areas colored grey are land.

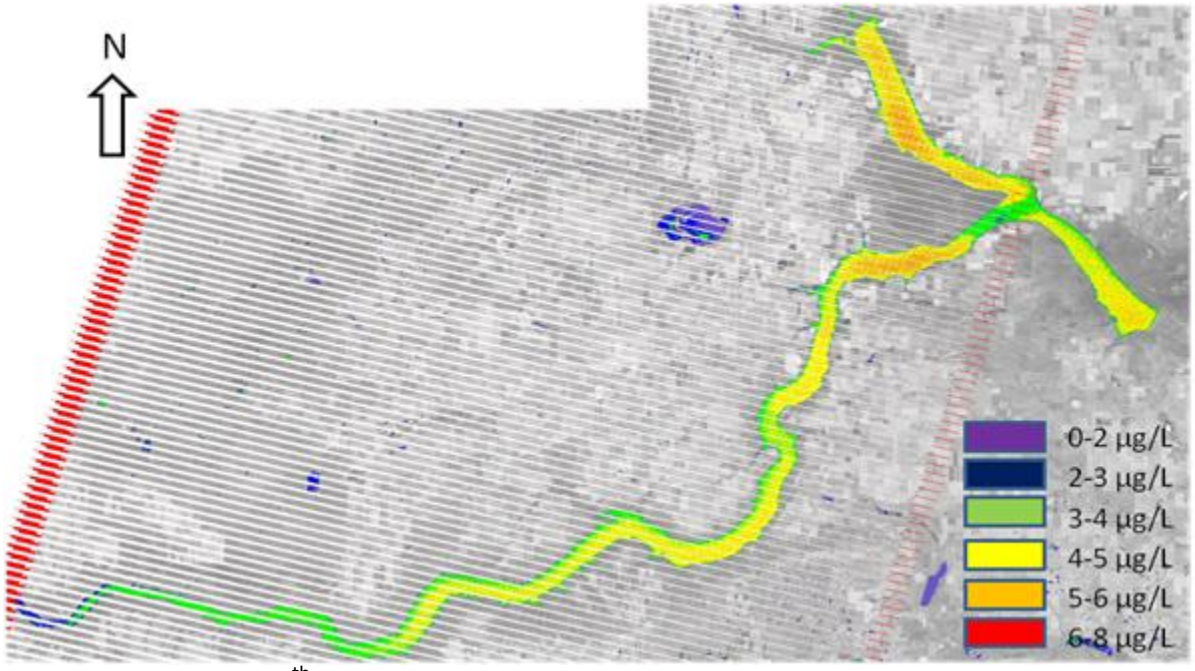

Fig. 2.12. September 27th, 2012 chlorophyll-*a* concentration. This image shows the changes in Chl-*a* distribution in LD throughout the year. In the fall, the highest Chl-*a* concentrations tend to be in the eastern arms while lower concentrations are found near the inflow. There was no algal bloom in the image, but Chl-*a* was highest in this image than any other throughout the year. Colored areas represent water, while areas colored grey represent land.

2.4 Discussion

2.4.1 Factors influencing Model Development

The models I developed for SDD and Chl-*a* concentration had lower coefficients of determination (R^2= 0.55 and R^2= 0.45 for SDD and Chl-*a*, respectively) values compared to other studies that have examined the same relationships (McCullough et al. 2012; Giardino et al. 2001; Allee and Johnson 1999). I attempted to use some of these models initially, but found they did not predict water quality well at Diefenbaker. Many of these studies used models that apply to only one or a few images. This method is useful for generating maps for a single image but requires ground reference data for each image they use. My models were generated from data acquired from different seasons, environmental conditions, and from separate years. As a result, they include a greater amount of variation than just a single or small sample of images. Therefore, they have a much greater scope and can be applied to any Landsat image acquired from Lake Diefenbaker. As such, they can acquire data from times where no field sampling occurred.

Time-lags between sampling and image acquisition were shown to cause a decrease in SDD model strength, but had no effect on Chl-*a* model strength. This result suggests that while the reservoir changes considerably over the course of an entire ice-off season, its day-to-day variation is relatively minor. Along with Kloiber et al. (2002) and Chipman et al. (2004), my research confirms that the slight decrease in model strength is a trade-off that is necessary to gather sufficient samples for a robust modeling algorithm. The more robust algorithm also allowed for inclusion of more data in my RMSE tests.

The multiple linear regression model for SDD used reflectance data from bands 4, 2 and 1. Band 4 was the primary component of the model, and reflectance in this band was

negatively related to SDD. In other words, shallow SDD values were related to increased reflectance values in band 4. This contribution is likely caused by the high flows that entered LD in during the field campaign (Fig. 2.3). The high flows arrived in late May and early June, and brought increased turbidity. Turbidity values increase from 10 NTU to over 200 NTU when high flows arrive in spring and summer (Hudson and Vandergucht, unpublished manuscript). This material is highly reflective and causes increases in the reflectance values (band 4) satellites while simultaneously reducing water clarity. When there is relatively low turbidity however, the light penetrates deeper into the water column and is not reflected. Because of this characteristic, band 4 is often used for identifying clear water (Carpenter and Carpenter 1983). The trends observed in SDD variation throughout the year are influenced by the sediment plume (Fig. 2.13) and it's progression through the reservoir.

Fig. 2.13. This Landsat 5 image shows the notable sediment plume that occurs in LD during spring high flow events (June 29th, 2011). Water appearing white to light grey in this image indicates high levels of turbidity and low SDD. The black water near the ends of the dam indicates relatively lower turbidity levels. White lines indicate the downstream progression of the sediment plume.

Band 3 did not affect SDD model strength, while bands 2 and 1 did. However, band 3 alone does explain 27% of the variation in SDD when modeled alone, indicating some redundancy with band 4 data. Bustamante et al. (2009) found a significant correlation between band 3 reflectance and turbidity, which can be directly related to SDD. This would suggest that band 3 and band 4 are detecting materials that have reflective properties that are similar across both bands, making them somewhat redundant at LD. Although minor in comparison to band 4, part of the models strength is derived from reflectance in bands 2 and 1, which may detect the small amount of algal turbidity in the water column (Brezonik et al. 2005).

The model I used to predict Chl-*a* concentration incorporated reflectance data from bands 4 and 3 (Fig. 2.4). The positive relationship with band 3 data can be explained by a Chl-*a* reflectance peak located at 690nm in the visible spectrum (Gurlin et al. 2011). When band 3 reflectance increases, predicted Chl-*a* concentration also increases. The band 4 portion of the Chl-*a* model is inversely related to reflectance; Chl-*a* concentration increases as the reflectance detected by band 4 decreases. The band 4 relationship helped to differentiate between Chl-*a* and non-algal turbidity. As the non- algal turbidity in the water column decreases, reflectance in band 4 decreases to nearly zero, and becomes less important for Chl-*a* estimation. Chlorophyll-*a* has its largest reflectance peak in the green light spectrum contained in Band 2, but I did not detect one in my study. The lack of a relationship may be due to turbidity in the reservoir, which causes reductions in the efficiency of blue and green satellite bands (Carder et al. 2004). Darecki and Stramski (2004) illustrated that typical Chl-*a* models which utilize band 2 and band 1 perform poorly in turbid waters, such as those present in spring and summer in LD. Tyler et al. (2006) used reflectance data from band 3 and suspended sediment concentration to

predict Chl-*a* concentration. Tebbs et al. (2013) found that bands 3 and 4 were also very successful in predicting Chl-*a* concentration in hypertrophic Lake Bogoria, Kenya. While both of the lakes in these studies differ from the environment at LD, they showed that it is possible to have functional predictive models that do not rely on band 2 information.

2.4.2 Secchi and Chlorophyll-a Concentration Trends

The predicted Secchi disk measurements varied considerably throughout the field seasons. Data extracted from the satellite imagery suggested that the study years exhibited similar patterns and trends in SDD, but there were not identical (Fig. 2.14).

The reservoir had relatively deep SDD measurements at the start of ice-free season (late April and early May). However, snowmelt and spring rainfall in the area surrounding the reservoir caused a slight decrease in water clarity in early May (Ashmore and Day 1988). When melt water from the Rocky Mountains arrived in early June, SDD became considerably shallower in the reservoir. Heavy rains in 2011 also caused a further reduction during this time. This pattern is typical of many reservoirs and can be caused by increases in colored dissolved organic matter or other suspended sediments (Kutser 2012). Reductions in water clarity begin near the SSR inflow and progress downstream into the reservoir throughout June. Once flow rates decline in July and August, SDD becomes deeper throughout the reservoir. The upstream regions of the reservoir (near Saskatchewan Landing) had the shallowest SDD readings. The areas near the Gardiner and Qu'Appelle Dam retain the deepest SDD readings year round.

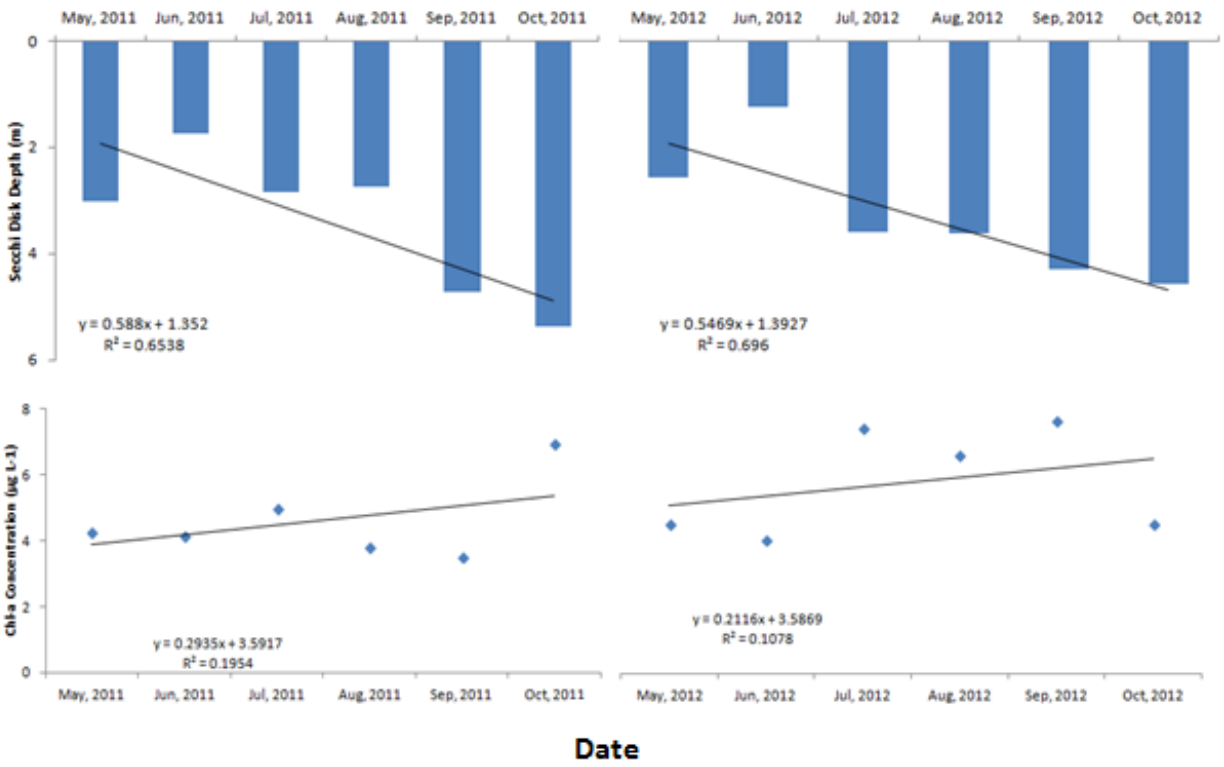

Fig. 2.14 Mean Chl-*a* concentration and Secchi disk depth during the 2011 and 2012 (May-October). This figure shows the trends that occur throughout the ice-off season of LD. Trends are similar between years the two years.

Predicted Chl-*a* concentrations in LD followed a less consistent pattern than SDD (Fig. 2.14). In 2011, the lowest mean Chl-*a* concentration occurred in August (3.81 µg L^{-1}), with a peak in October (6.94 µg L^{-1}). In 2012, Chl-*a* concentration was lowest in June (2.94 µg L^{-1}), and increased slightly throughout the field season until it peaked in September (5.89 µg L^{-1}). Spatially, Chl-*a* concentration was greater in the Gardiner and Qu'Appelle arms of the reservoir. During the high flows present in the spring (May-June), Chl-*a* concentration was highest within the sediment plume brought in by high flows, and slightly lower in the arms of the reservoir.

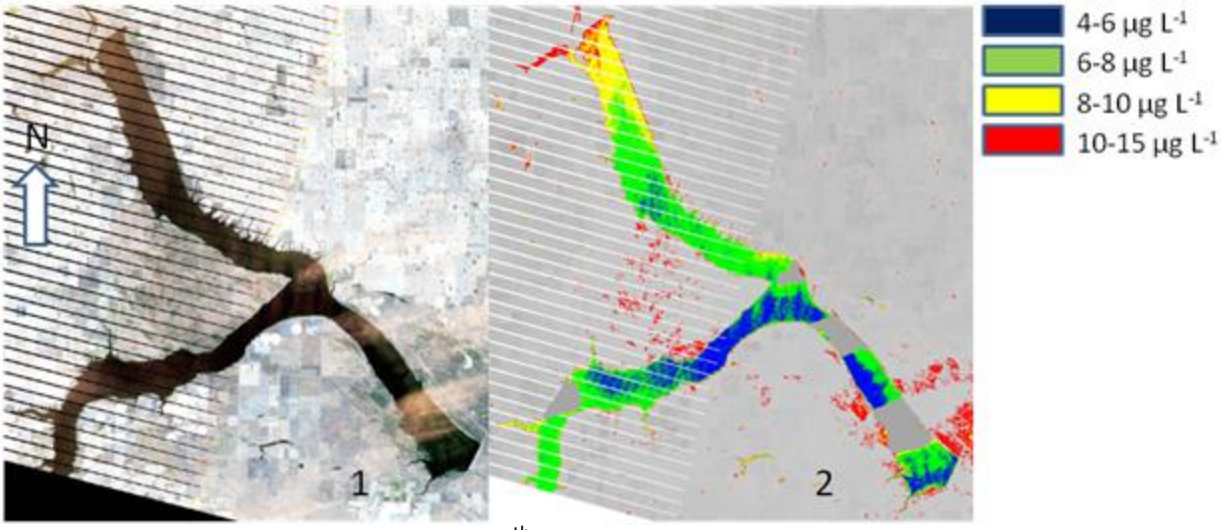

Fig. 2.15. Algal bloom on September 25th, 2011. The natural color image (Panel 1) shows a green scum of water on the eastern portion of the reservoir in the Qu'Appelle arm and near the northern half of the Gardiner arm. The colored image (Panel 2) reflects the models ability to also detect this algal bloom. Note that the grey areas represent clouds that covered portions of the reservoir, or land. Colored areas represent different concentrations of Chl-*a*.

The largest algal bloom event captured by the satellite imagery during the 2011 and 2012 field seasons was observed in the Qu'Appelle and Gardiner arms on September 25th, 2011. This bloom was signaled by a visible algal scum on the water surface, and higher concentrations of Chl-*a* when compared to the rest of the month. In addition, high values of band 3 reflectance compared to nearby waters were detected from the region. The image was partially covered by clouds and portions of the reservoir could not be imaged (Fig. 2.15). Field sampling performed the next day (September 26th, 2011) showed that the surface scum was not present. The greatest concentrations of Chl-*a* were observed in September and October. The Qu'Appelle arm of the reservoir tended to have the highest concentrations of Chl-*a*. Both of these observations were likely caused by sporadic algal blooms in the late fall in the Qu'Appelle arm of the reservoir. This portion of the reservoir is shallower, and the water is at risk of stagnation (Costa 2011). In addition, high temperatures and calm weather common during this

time of the year make it an ideal location for algal blooms (Paerl and Huisman 2008). However, algal blooms were not observed in all fall imagery, indicating that the environmental and internal lake conditions necessary for algal blooms occur only sporadically in the reservoir.

2.4.3 Causal Factors in Predicted Water Quality Trends

Spring inflow from this river is likely one of the most important events during the ice-off season because 98% of the water in LD comes from the SSR. The inflow brings in a large sediment plume that travels down the reservoir until it recedes or settles on the reservoir bottom in July and August. The patterns in SDD and Chl-*a* concentration are also considerably affected by this inflow pattern. This pattern is common in many reservoirs (Poff et al. 1997). Both of my study years were atypically high flow years and therefore the changes in water quality may not be typical. However, the pattern observed in these two variables is likely similar from year to year, and simply the magnitude changes. The patterns of water clarity and Chl-*a* concentration observed at LD illustrate the complexity of this reservoir. These patterns also suggest that using a single satellite image or single date would be ineffective at characterizing LD water quality. Therefore the use of a model that incorporates data from multiple dates and environmental conditions not only makes the model more robust, but also more representative of the reservoir.

Yearly sediment plumes bring large amounts of nutrients into the system, but also limits the amount of light that can enter the water column. Therefore algae are likely light limited, causing Chl-*a* to decline as well. My results showed a positive relationship between Chl-*a* and SDD, which suggests that the non-algal turbidity plays a greater role in reducing water clarity than does algae concentration. This relationship is atypical for most aquatic systems (Carlson

1977). However, Canfield Jr. and Bachmann (1981) found that this the pattern seen here is more common in artificial lakes. Lind (1986) found that in turbid reservoirs, a relationship where SDD became deeper when Chl-*a* increased is possible. Lake Diefenbaker can be considered a turbid reservoir during high flow events. Once the turbidity and sediment settles to the bottom or is flushed out of the system, light can penetrate the water column. The increased light availability stimulates algal growth. Leftover nutrients brought into the reservoir after spring high flow events may also help to stimulate this algal growth (Schindler et al. 2012).

2.4.4 Limitations of Models and Imagery

Certain natural phenomena have led to decreases in my model's strength. One such phenomena is sun glint, which has a considerable and unpredictable effect on the reflectance detected by the satellites. This glint is caused by both large waves, and solar zenith angles below 30 degrees (Chen et al. 2011). For the vast majority of my images however, only high waves would be a contributor of solar glint because the solar zenith angle at the time of imaging was almost always above 30 degrees. High winds also have the ability to mix a water column, and vertically disperse surface algae into deeper water (Kahru et al. 1993). Rapidly changing winds could create a sizeable difference in near-surface Chl-a concentrations between imaging time and water collection time.

The Chl-*a* model used in this study tended to underestimate actual Chl-*a* concentrations. Furthermore, this underestimation was greater when Chl-*a* concentrations were high. This is likely because high Chl-*a* concentrations were not included in the development of the model. As such, the model may be unable to accurately quantify the severity of algal blooms at LD. This model however, is still very useful in identifying where and when large algal blooms take

place. Future work will attempt to reduce the error in the Chl-*a* model while maintaining its ability to be applied to any image.

The temporal resolution of the Landsat satellites makes it difficult to identify quickly-evolving events. Although the reservoir is located in a location that facilitated 8-day resolution, this study is better suited for observing the reservoir at a monthly or bi-weekly frequency, as good quality and cloud-free images are not captured at a consistently higher resolution. While this resolution is effective for measuring long-term trends in water quality, it may not be able to capture events that are short-lived in nature. In addition, it is possible that blooms smaller than the minimum detection size for Landsat satellites (15m) occurred at LD. However, small blooms might also be environmentally non-significant, so switching to a satellite with more precise spatial resolution might be unnecessary.

One of the most notable limitations in this study is that the Chl-*a* model can only detect algal concentrations that are on the surface or near the surface. Since the amount of light reflected from deeper waters is negligible, submerged algal blooms are difficult to detect using current methods of satellite image analysis. While algal activity is presumably greatest in the upper portions of a water column, there is evidence of algal blooms forming lower in the water column (Paerl et al. 2001).

2.4.5 Future Directions

This research could be applied to LD to reduce the cost and effort of monitoring this large reservoir. However, further improvements to this study are needed before it can take the place of traditional monitoring. An advisable next step would be to increase the explanatory power of the predictive models. Additional field sampling may incorporate greater algal

concentrations and SDDs and lead to greater model applicability. In addition, developing relationships between satellite digital data and additional water quality variables such as temperature, turbidity, suspended sediment concentration, specific algal pigments, and more would allow for greater dependence on satellite imagery in the place of field sampling.

The launch of Landsat 8 has already increased the frequency of good quality images that are acquired of LD. Furthermore, converting the models I generated in this study to the new 16-bit format of Landsat 8 will allow for new data to be extracted from these images. The launch of this new satellite ensures that the Landsat program and the models generated in this study will be useful for several years into the future.

2.5 Conclusions

Models that can predict chlorophyll-*a* concentrations and Secchi disk depth were developed for LD using Landsat satellite imagery. There were significant relationships between Chl-*a* concentration and SDD in both predicted and actual data. This allowed me to conclude that decreases in water clarity are not caused by increases in algal concentrations. The time-lag analysis showed that as time between sampling and image acquisition increased, the explained variation in the SDD model decreased a small amount, while the explained variation in the Chl-*a* model did not change considerably. I can therefore conclude that the day-to-day variation in the reservoir is relatively low. Model accuracy was assessed by comparing predicted SDD and Chl-*a* concentration to actual values recorded in the field. There was a strong correlation between predicted and actual in both models, and they had an RMSE of 1.01m and 2.54 $\mu g\ L^{-1}$ for SDD and Chl-*a* respectively. The SDD model predicts well at all depths of SDD, while the Chl-*a* model underestimates actual concentrations. Despite this consistent

underestimation, the model can still accurately identify the presence and extent algal blooms. I also concluded that high flow events arriving from the Rocky Mountains in the spring have a sizeable influence on the water quality of the reservoir. Very high flows into LD were recorded for 2011 and 2012. These high flows in spring bring a large load of sediment, nutrients, and other debris into the reservoir. The broad range of images that these models can be used on make them attractive for future use on LD. Although they explain slightly less variation when compared to comparable studies, they can be applied to a greater number of Landsat images. As such, these models can be used to complement or reduce the amount of field sampling that is necessary to monitor this large prairie reservoir.

Chapter 3: A 29-Year Assessment of the Water Clarity and Chlorophyll-*a* concentration Trends in a Large Reservoir: Investigating Spatial and Temporal Changes using Landsat Imagery[2]

3.1 Introduction

Responsible management of natural ecosystems is critical in order to maintain the economic, recreational, and cultural benefits that they provide. Ecosystems can be managed more effectively if long-term monitoring information is available. Short-term monitoring often does not accurately detect gradual changes in an ecosystem, or identify multi-year or multi-decadal patterns (Magnuson 1990). As such, long term monitoring programs are critically important for detecting environmental change. Long-term monitoring has been fundamental for understanding the effects of climate change (Dawson et al. 2011; Keeling et al. 1995) and acid rain (Likens and Bormann 1974). However, the cost of maintaining personnel and equipment for monitoring programs can quickly exceed budgets. Therefore, alternative methods of monitoring are sought.

Remote sensing is effective for monitoring many aspects of the natural environment. Orbital satellites are a particularly useful alternative to field sampling for certain applications. They have the advantage of a wide field of view, frequent revisit cycle, and lower cost compared to a long-term field campaign. Satellites have been used for a number of long-term studies, e.g., evaluating forest fire history (Russell-Smith et al. 1997), long-term lake water clarity (McCullough et al. 2013) and long-term chlorophyll-*a* concentration (Binding et al. 2011). In addition, satellite data is often archived, and therefore can be used for hindcasting. This in

2 **Note** This chapter of my thesis has been accepted for publication in the Journal of Great Lakes Research. Yip, H.D., Johansson, J.J, and Hudson J.J. In Press. A 29-Year Assessment of the Water Clarity and Chlorophyll-*a* concentration of a Large Reservoir: Investigating Spatial and Temporal Changes using Landsat Imagery.

turn can be used to approximate field data if appropriate and precise models are developed. The Landsat program has been used extensively for hindcasting (Wulder et al. 2012). In 2008, all Landsat imagery became free-to-use, and as a result, application of the imagery has increased (Woodcock et al. 2008). Since the first Landsat platform was activated in 1972, a total of eight satellites have been launched under the Landsat program. While only two satellites are functional today, they continue to collect data and store it in an open access archive maintained by the United States Geological Survey (USGS). Landsat 5 and 7 were developed for terrestrial studies, but their broad spectral bands have allowed them to be adapted for aquatic use as well. Many studies have generated models from Landsat that are used to predict water quality (Karakaya et al 2011; Wang et al 2004; Brivio et al 2001; Baban 1993). However, only a few studies have used Landsat to predict historical water quality data (Barnes et al. 2014; Duan et al. 2009; Olmanson et al. 2008; Sass et al 2007).

Chlorophyll-*a* (Chl-*a*) concentration and Secchi disk depth (SDD) have been used extensively to characterize water quality. These variables are easy to collect and their relationship with the trophic status of lakes (Carlson 1977) makes them excellent indicators of ecosystem function. These variables often can be linked to other water quality indicators, such as phosphorus concentration (Torbick et al. 2013; Dillon and Rigler 1974). Chlorophyll-*a* concentration is also a proxy for algal biomass and harmful algal blooms (Paerl and Huisman 2008; Anderson et al. 2002). It is also a key indicator of pollution, as inputs of certain nutrients tend to cause large increases in algal populations (Carpenter et al 1998; Schindler 1974). Secchi disk depth is a measure of water clarity and can be used to estimate lake productivity (Preisendorfer 1986). In addition, a change in Chl-*a* or SDD is accompanied by changes to the

visual appearance of the water. As such, fluctuations in Chl-*a* and SDD also cause changes in the reflective properties of the water. This property allows satellite imagery to assess changes in SDD and Chl-*a* concentration.

Lake Diefenbaker (LD) is a large reservoir located in southern Saskatchewan, Canada. The reservoir is approximately 225 km long with a mean width of 2-3 km. The reservoir has a surface area of approximately 430 km and shoreline length that exceeds 800 kilometers. The reservoir began to fill once the construction of two large dams was completed in 1967. The Gardiner Dam on the north-east end of the reservoir regulates flow into the South Saskatchewan River (SSR), while the Qu'Appelle dam controls flow into the Qu'Appelle River. The Gardiner Dam has a hydroelectric station, and the majority of water that leaves through the reservoir passes through this dam. Water levels in the reservoir can vary by up to seven meters throughout the year, with highest levels occurring after high flows in spring and lowest levels in mid-winter (Bogard et al. 2012). The majority of water entering LD (98%) enters from the SSR which lies upstream of the reservoir. The SSR's flows originate mainly from precipitation and glacial melt in the Rocky Mountains, with a smaller contribution from local precipitation and runoff (Pomeroy et al. 2005). Flows into the SSR can be large and can cause considerable flooding in some years. The reservoir is used for drinking water, recreation, hydroelectric power generation, irrigation, fish farming, and more. Several small communities surround the reservoir, but the vast majority of the reservoir is surrounded by agricultural land. Much of it is used for cattle grazing, but there is also cropland adjacent to the reservoir.

Lake Diefenbaker is an important reservoir in the province, but has been understudied during its lifetime. This study is a part of a larger research effort aimed at better characterizing

Lake Diefenbaker for effective future management. There were three objectives in my study. First, I wanted to examine the historic spatial and temporal changes in chlorophyll-*a* concentration or Secchi disk depth from 1984 to 2012 with satellite imagery. Second, I wanted to determine if the models developed using this imagery are an accurate tool for hindcasting water quality data by comparing predicted and actual historical data. Third, I wanted to investigate the frequency and location of historic algal blooms to determine if blooms were increasing over time; local residents have suggested blooms have become more prevalent.

3.2 Methods

3.2.1 Image Preprocessing

Landsat imagery was obtained from the USGS Global Visualizer website (glovis.usgs.gov). Lake Diefenbaker lies along paths 37 and 38, and rows 24 and 25 of the WRS-2 orbit. Two images from the same path, but different rows from each sampling day were combined into a single image for analysis because the reservoir's size exceeds a single image. The location of the reservoir allowed images to be taken every 8 days instead of the typical 16 day revisit cycle. On days when path 38 images were used, a portion of the Qu'Appelle arm was outside the satellite path and was not imaged. The portion is small, and did not cause significant data loss. Continuous data collection for LD did not begin until 1984, although Landsat 5 was launched in 1982. As such, my study examined a 29-year period of imagery from 1984-2012.

Satellite imagery was downloaded in a Geotiff format and then converted into a useable format in PCI Geomatica (Version 10.3). Images were geometrically corrected by the USGS. The images were then radiometrically and atmospherically corrected. Atmospheric correction

was performed using an improved dark-object subtraction technique (Chavez 1988). A 3x3 moving average filter was used to smooth data and reduce the effect of pixels affected by wave action, or recording errors by Landsat sensors before data extraction. In addition, slight orbital movement of the Landsat satellites caused pixels to occasionally fall near the edge of two pixels, and smoothing reduced error caused by this movement.

3.2.2 Data Extraction Schedule

Every cloud-free image acquired by Landsat 5 and 7 since 1984 could have been processed and modeled, but the frequency of available data was not consistent throughout this time. Therefore, in order to get a consistent and manageable dataset, I limited my image analysis to a once-monthly extraction from May to October (1984-2012). Mid-monthly images were used; however, if such an image was unavailable the next quality image that was used instead. I extracted information from sixteen sites that were spaced throughout the reservoir. These sites were chosen because they are representative of the entire reservoir (Fig. 3.1). The sites were selected to avoid scan-line corrector (SLC) errors on the Landsat 7 ETM+ sensor (Fig. 3.10).

3.2.3 Image Acquisitions

I reviewed 272 individual images and combined these to form 136 whole-reservoir images. For the period of 1984-1999, only Landsat 5 was operational. From 1999 to 2011, Landsat 5 and 7 were both operational. In 2012, only Landsat 7 collected imagery. On two occasions in 1989, Landsat 4 TM images were obtained because Landsat 5 imagery was unavailable. Landsat 4 and 5 share identical instruments, so no additional steps were necessary for analysis. Most of the months in my study had images where data could be extracted (136 of

164 months, 83%). Cloud cover or image absence were the primary reasons for not obtaining an image in a given month. In some cases, interference from cloud cover allowed only partial data extraction from an image.

3.2.4 Model Generation

In situ sampling and satellite image acquisition took place in May to October in 2011 and 2012. Models were generated to predict Chl-*a* concentration and SDD at LD using the acquired satellite data. These models were generated from a dataset that included multiple dates and environmental conditions, allowing for a single model for each variable. These models are described in equations 3.1 (SDD) and 3.2 (Chl-*a*) below, where *a* is the reflectance in Band 4, *b* is the reflectance in Band 2, *c* is the reflectance in Band 1, and *d* is the reflectance in Band 3.

Equation 3.1: $\text{SDD (m)} = (-126.54*a) - (5.74*b) - (8.23*c) + 4.18$

Equation 3.2: $\text{Chl-}a\ (\mu g\ L^{-1}) = (-115.95*a) + (19.31*d) + 4.56$

The predicted data from these models was significantly related to the reference data that was obtained from field sampling (SDD, $p<0.05$, $R^2=0.62$; Chl-*a*, $p<0.05$, $R^2=0.56$ (model I regression)). The models also had a comparable root-mean squared error (RMSE) to other studies of this kind (SDD= 1.01 m and Chl-*a* = 2.54 $\mu g\ L^{-1}$). Data used to assess RMSE was independent and not used in model development. The RMSE estimate does not have a threshold, but it can be compared to other studies to assess the performance of models. The Chl-*a* model tended to underestimate the actual chlorophyll concentration (Fig. 2.5, Panel 2). As the predicted Chl-*a* increased, the error between predicted and actual concentrations also increased. However, algal blooms were still detected despite this underestimate. There was no

predictive large predictive bias in the SDD model (Fig. 2.5, Panel 1). These models were then applied to archived imagery to satisfy objective one.

Fig. 3.1. Data extraction sites at Lake Diefenbaker, SK from Landsat 5 or 7 satellites. Each point represents a site where water quality information was measured from the satellites. Site numbers are arranged such that lower numbers were closest to the inflow (SSR), while the higher numbers are closest to the outflows (Gardiner and Qu'Appelle dams). The inset at top left indicates the reservoir's location in SK. Local areas of interest are also labeled on the figure.

3.2.5 Archive Analysis Methods

Figures were generated and statistical analysis was performed in the R statistical environment (Version 2.15.2). I investigated spatial and temporal trends of SDD and Chl-*a* concentration. Locally weighted scatterplot smoothing (LOESS) was used to identify trends in mean temporal and spatial SDD and Chl-a concentrations. A regime-shift analysis (RSA) was used to determine if long-term trends in the reservoir were significant (STARS sequential t-tests; Rodionov and Overland, 2005). This type of RSA is more effective at correctly identifying regime shifts near the end of a time-series where data is limited (Rodionov 2004). A regime shift was defined as considerable and persistent change in the reservoir's mean yearly SDD or Chl-*a* concentration from one state to another. Mean annual values of SDD and Chl-a were

tested for regime shifts using a threshold significance level of p=0.05 and a cut-off length of L= 5 years, similar to a study on Lake Simcoe (North et al. 2013). If a regime-shift was detected, the mean Chl-*a* and SDD values for the time period were reported both before and after the shift, to indicate which direction the water quality variables had shifted.

My predictive models were able to accurately predict of Chl-*a* and SDD during modeling years (2011 and 2012) when compared to similar studies (Chapter 2, section 2.3.6). However, I also wanted to test their ability to predict historical water quality. Data from a study conducted in 1984-1985 by Saskatchewan Environment and Public Safety (SEPS, 1988) and a dataset from the province of Saskatchewan (Pam Minifie, Drinking Water and Wastewater Management Division, Water Security Agency, personal communication) were used in this assessment. Historic field data that was within five days of a good quality historical image was used in the assessment. Linear regression analysis (model II) and RMSE was used to assess model performance and fulfill the second objective of this study.

To satisfy the third objective of my study, I investigated the frequency and seasonal timing of algal blooms. I classified blooms by identifying rapid increases in band 3 reflectance, coupled with decreases in band 4 reflectance. True color images were used to confirm the presence or absence of an algal bloom. I explored a number of morphometric (such as reservoir depth and flow path) and environmental factors (such as wind speed and light limitation) that are known to influence the appearance of algal blooms (Paerl 2008).

3.3 Results

3.3.1 Historic SDD and Chl-a Modeled Results

The predicted mean Secchi disk depth was 4.42m (range: 0.07 m- 6.86 m, 95% CI ± 0.05m) and the predicted mean Chl-*a* concentration was 5.93µg L^{-1} (range: 1.42 µg L^{-1} – 12.54 µg L^{-1}, 95% CI ± 0.09 µg L^{-1}) during the 29-year study period. There was a positive correlation between predicted Chl-*a* concentration and SDD (n =2040). This suggests that Chl-*a* concentration actually increased with water clarity.

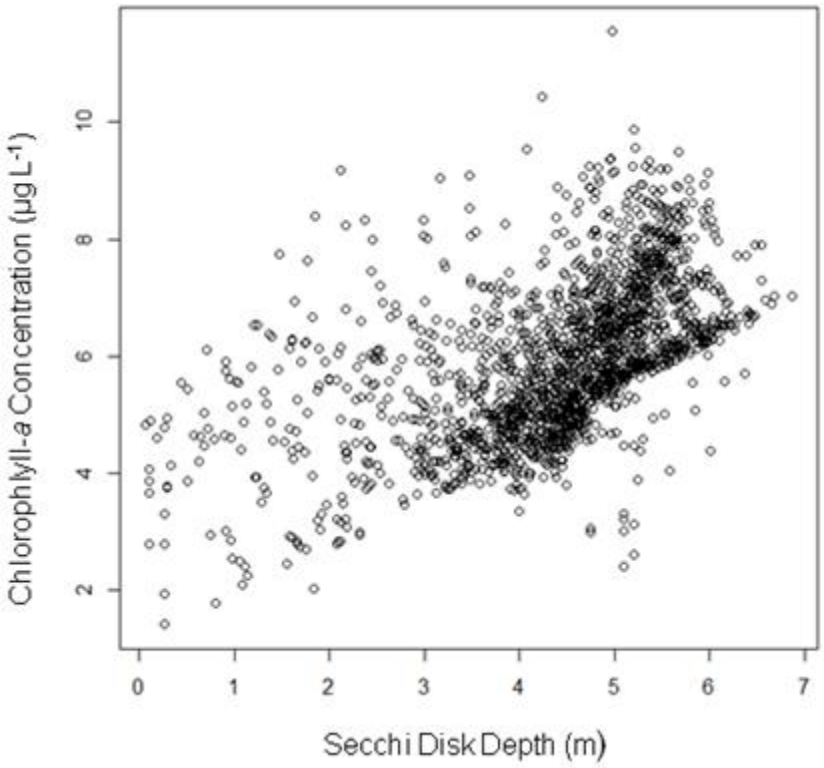

Fig. 3.2. Relationship between predicted SDD and predicted Chl-*a* concentration for Lake Diefenbaker (1984-2012). There is a positive correlation here that suggests Chl-*a* concentration increases with water clarity.

3.3.2 Agreement between Predicted and Actual Chlorophyll-a and Secchi Disk Depth

There was a significant relationship between actual and predicted historic SDD values (n=39, p <0.0001 R^2=0.84, model II regression). Root-mean-squared error was 0.85m for SDD

(Fig. 3.3, panel 1). Actual and predicted Chl-*a* concentration values had a higher RMSE (1.34 µg L^{-1}) and the relationship was weaker, but still significant (n=23, p <0.0001, R^2=4.8X10^{-5}, model II regression; Fig. 3.3, panel 2). The SDD model had almost no predictive bias, but the Chl-*a* model tended to underestimate actual Chl-*a* concentrations.

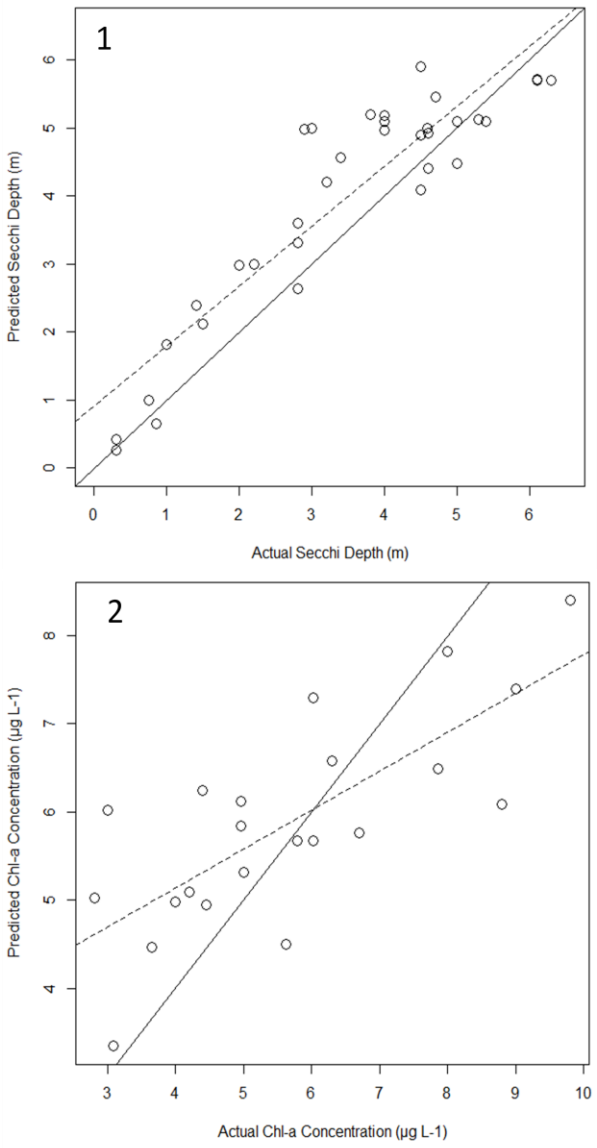

Fig. 3.3. Reference vs. predicted SDD (Panel 1) and Chl-*a* concentration (Panel 2). The 1:1 line represented by the solid line, illustrates the relationship if predicted values were identical to observed values. The dashed line represents the actual relationship between the satellite predicted values and actual values (R^2=0.84, RMSE=0.59m for SDD, 0.57, RMSE=1.59 µg L^{-1} for Chl-*a* concentration, model II linear regression).

3.3.3 Temporal Changes in Water Quality from 1984-2012

Two regime shifts were detected in both water quality variables during the study period (n=29, *p*=0.05, STARS RSA). Regime shifts occurred in 1992, and again in 2011 for both variables. The first SDD regime (1984-1991) had a mean depth of 4.80m. The second regime's mean declined to 4.32m during 1992-2010. The third regime had a further decline, with a mean of 3.40m in 2011-2012. For Chl-*a*, the first regime had a mean of 7.05 µg L^{-1} (1984-1991). There was a decrease in the mean for the second regime (1992-2010) to 5.53 µg L^{-1}. The final Chl-*a* regime had a mean of 4.64 µg L^{-1} for the final two years of the study (2011-2012).

Monthly mean SDD values were deepest in October and shallowest in June (Fig. 3.4, upper panel). Chl-*a* concentration was greatest in October and lowest in June (Fig. 3.4, lower panels). Variation was large from year-to-year, so mean trends were analyzed instead of individual years. The regime shifts are well depicted in the pattern in mean yearly SDD (Fig. 3.5, upper panel). Monthly trends in SDD were generally similar to the yearly trend in shape with the exception of October (Fig. 3.5, lower panels). The regime shifts in Chl-*a* could also be identified graphically, and show a general decline in overall Chl-*a* concentration. Monthly trends in Chl-*a* were very similar to the yearly trend.

3.3.4 Spatial Changes in Water Quality from 1984-2012

Mean seasonal SDD was shallowest at the upstream section of the reservoir, but was relatively consistent throughout the rest of the reservoir (Fig. 3.7, panel 1). Mean seasonal Chl-*a* concentration was spatially similar in most sites, except for slightly greater concentrations in the downstream sites (12-16, Fig 3.7, panel 2). The declining trend in water clarity is similar at all sites (Fig. 3.8), and is similar in shape to the mean trend (Fig. 3.5, upper panel). However,

water clarity in downstream sites declined less than water clarity in upstream sites. Spatial changes in Chl-*a* concentration also followed a declining curve, but this decline is spatially consistent throughout the reservoir (Fig. 3.9).

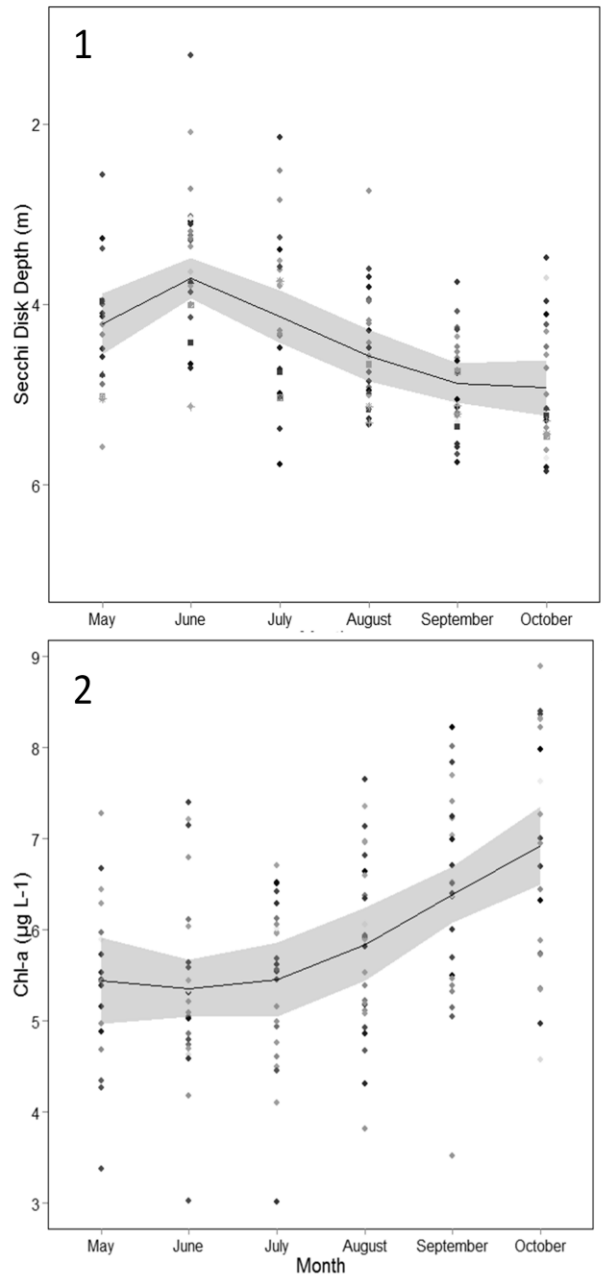

Fig. 3.4. Mean monthly SDD (panel 1) and Chl-*a* concentration (panel 2). In both panels the thick dark line represents a LOESS fit to data from all years. Each data point represents a single monthly mean in one year. The y-axis in panel 1 is reversed to represent the SDD below the water surface.

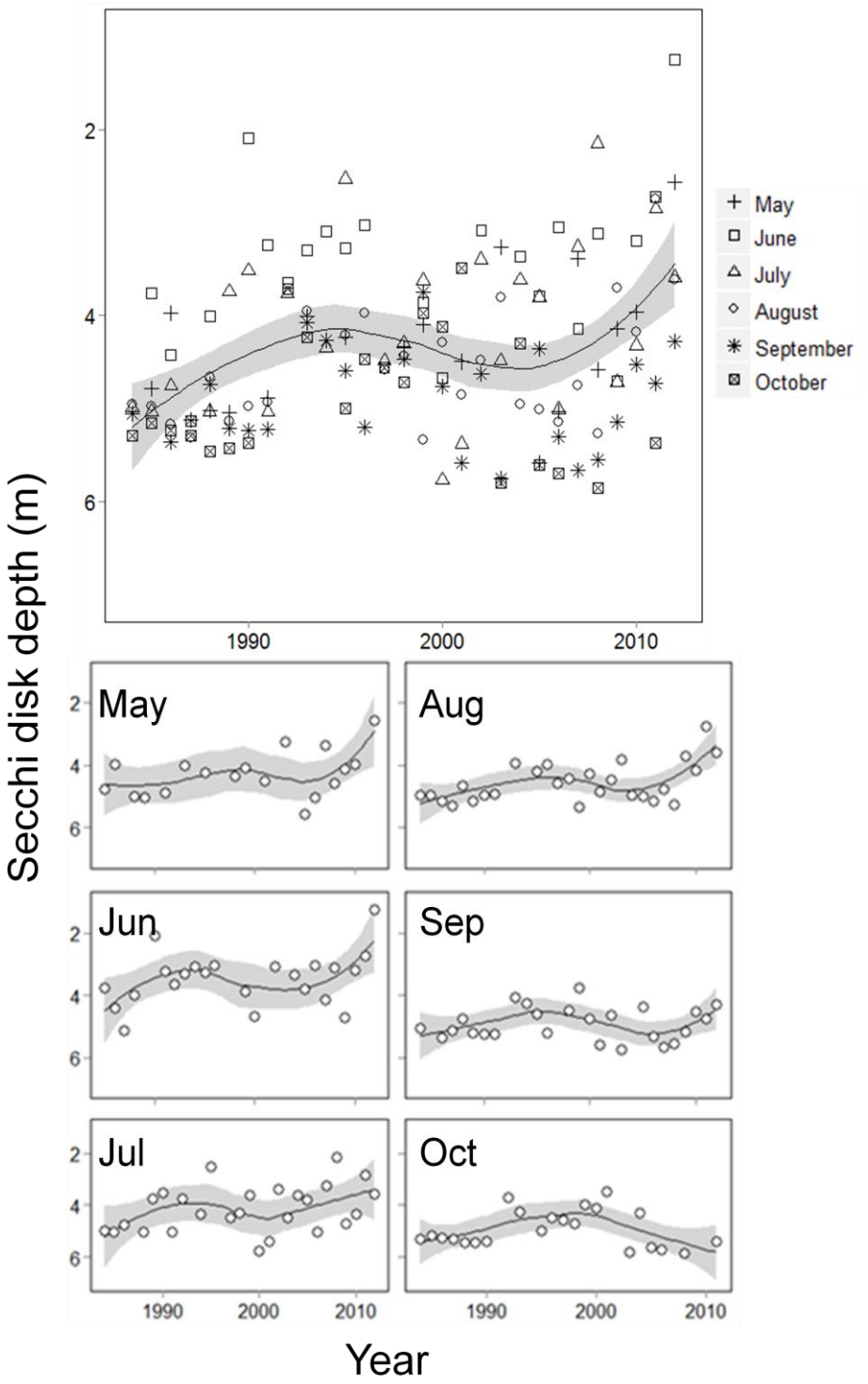

Fig. 3.5. Mean yearly Secchi disk depth 1984-2012 (upper panel) and monthly mean SDD (lower panels) in Lake Diefenbaker. A decreasing trend in water clarity as measured by SDD over the study period is evident. Each relationship is fitted to a LOESS smoothed line and the gray area represents a 95% confidence interval. The lower panels show the individual contribution of each month. A single point in each panel represents a single monthly mean. The y-axis is reversed in each to represent depth.

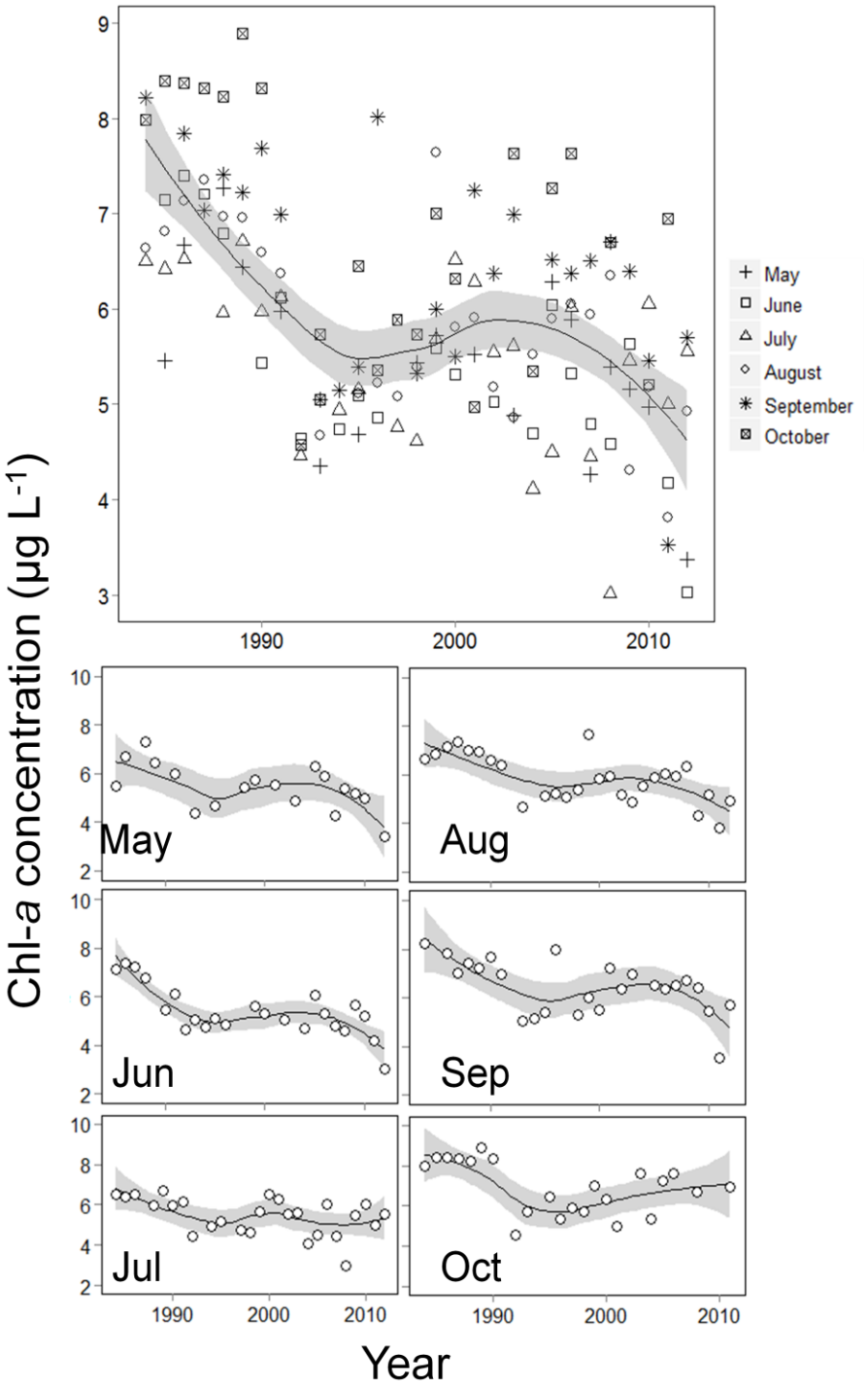

Fig. 3.6. Mean yearly Chl-*a* concentration 1984-2012 (upper panel) and monthly mean Chl-*a* concentration (lower panel) in Lake Diefenbaker. A decreasing trend in chlorophyll-*a* concentration is notable over the study period. Each relationship is fitted with a LOESS smoothed line and the gray area represents a 95% confidence interval. The lower panels show the individual contribution of each month in the upper panel. A single point in each panel represents a monthly mean from a single year.

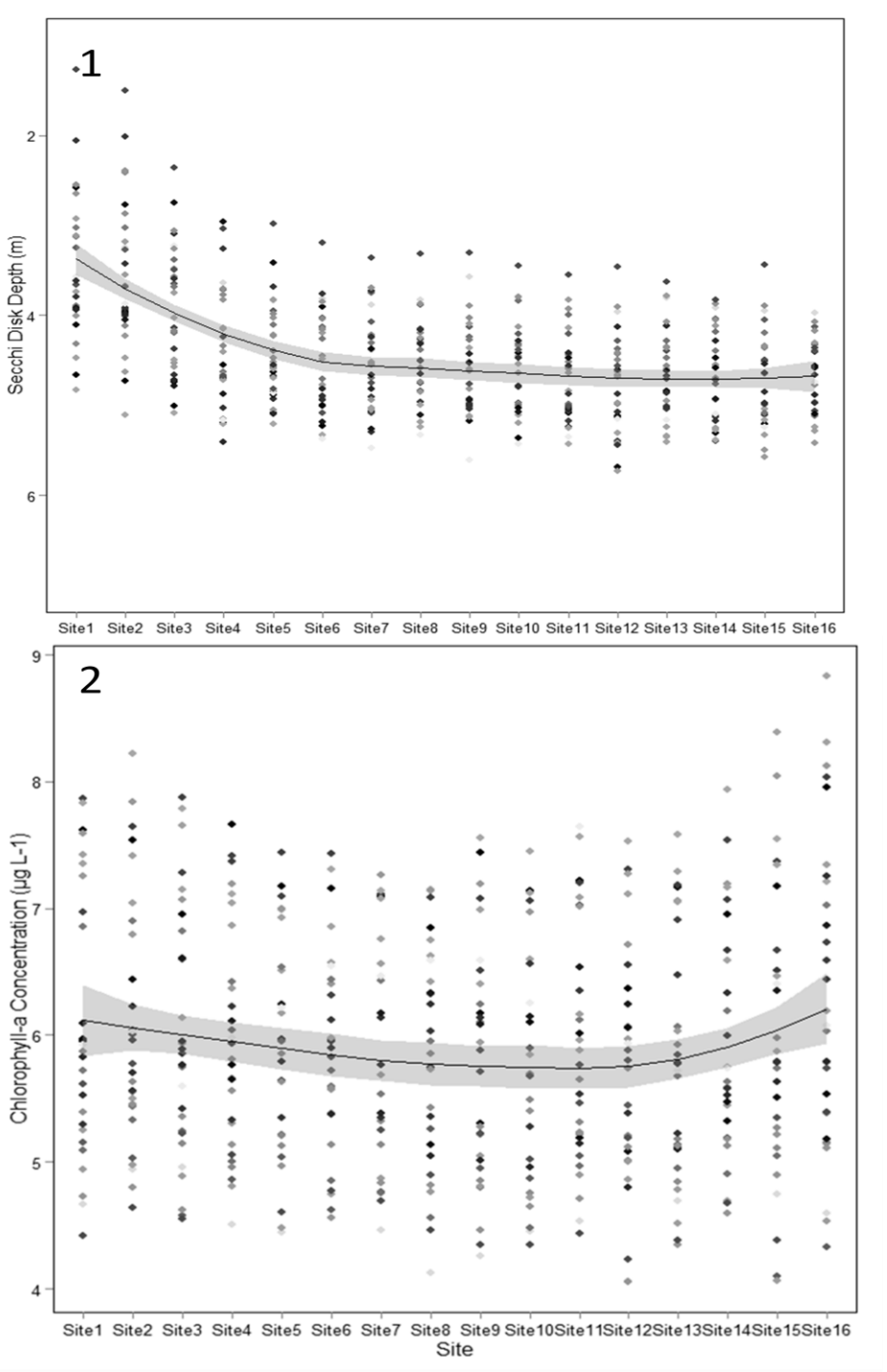

Fig. 3.7. Mean site SDD and Chl-*a* concentration over the 29-year study period. Panel 1 illustrates SDD, while panel 2 shows Chl-*a* concentration. The thick dark line represents a LOESS regression line. Individual points represent a yearly mean for a single site. Note the y-axis is reversed in panel 1, with deeper Secchi disk values on the lower end of the graph. In both graphs, sites are presented so that Site 1 is closest to the inflow of LD, while 12-16 are in the arms of the reservoir.

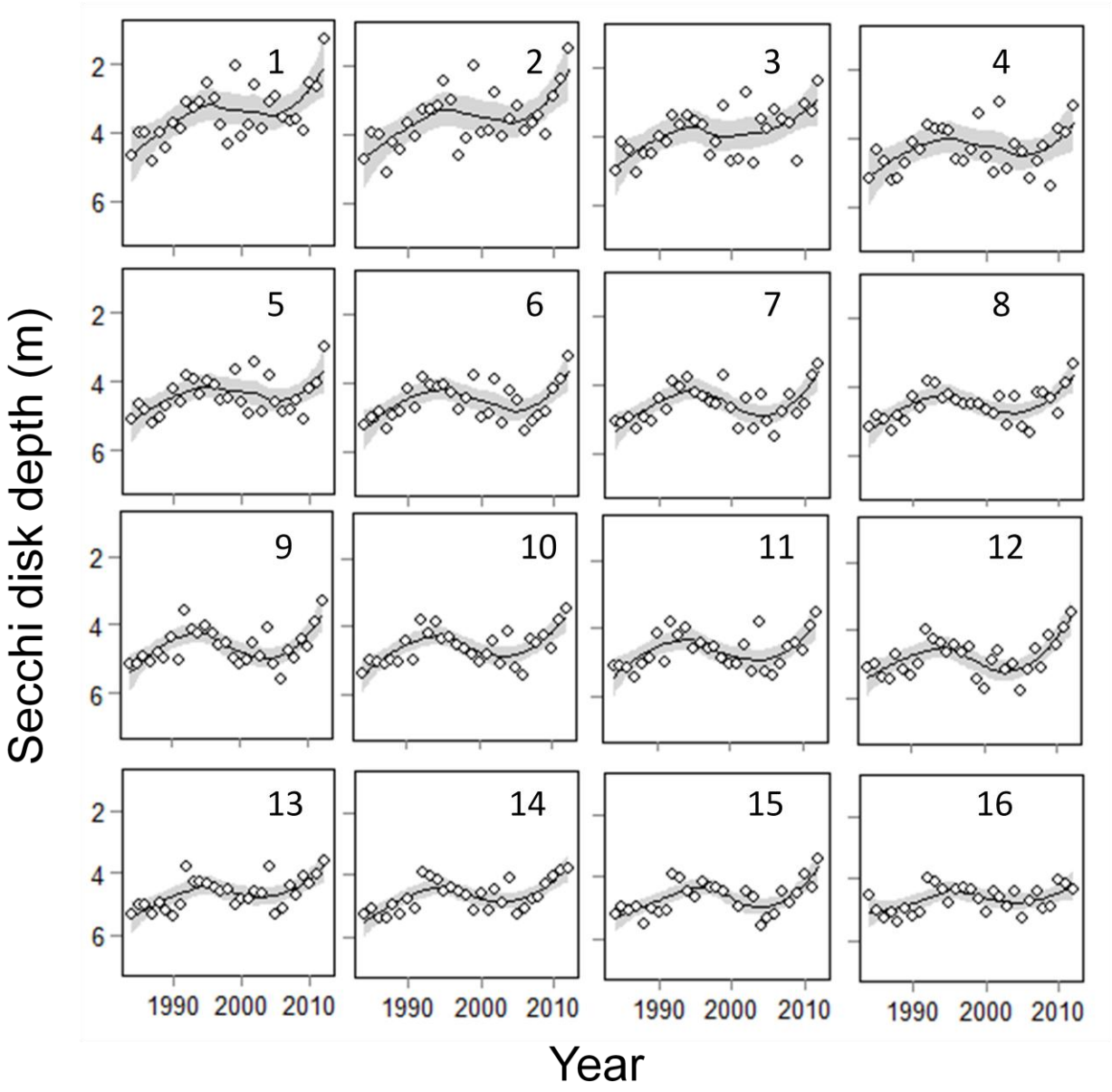

Fig. 3.8. Relationship between SDD and year at each site. Sites closer to the inflow (lower numbered sites) had larger decreases in water clarity, while sites downstream and closer to the dams (higher number sites) have remained relatively unchanged. Each relationship is fitted to a LOESS smoothed line, and the gray areas represent 95% confidence intervals. The y-axis is reversed in each to represent depth. A single point in each panel represents a monthly mean from a single year.

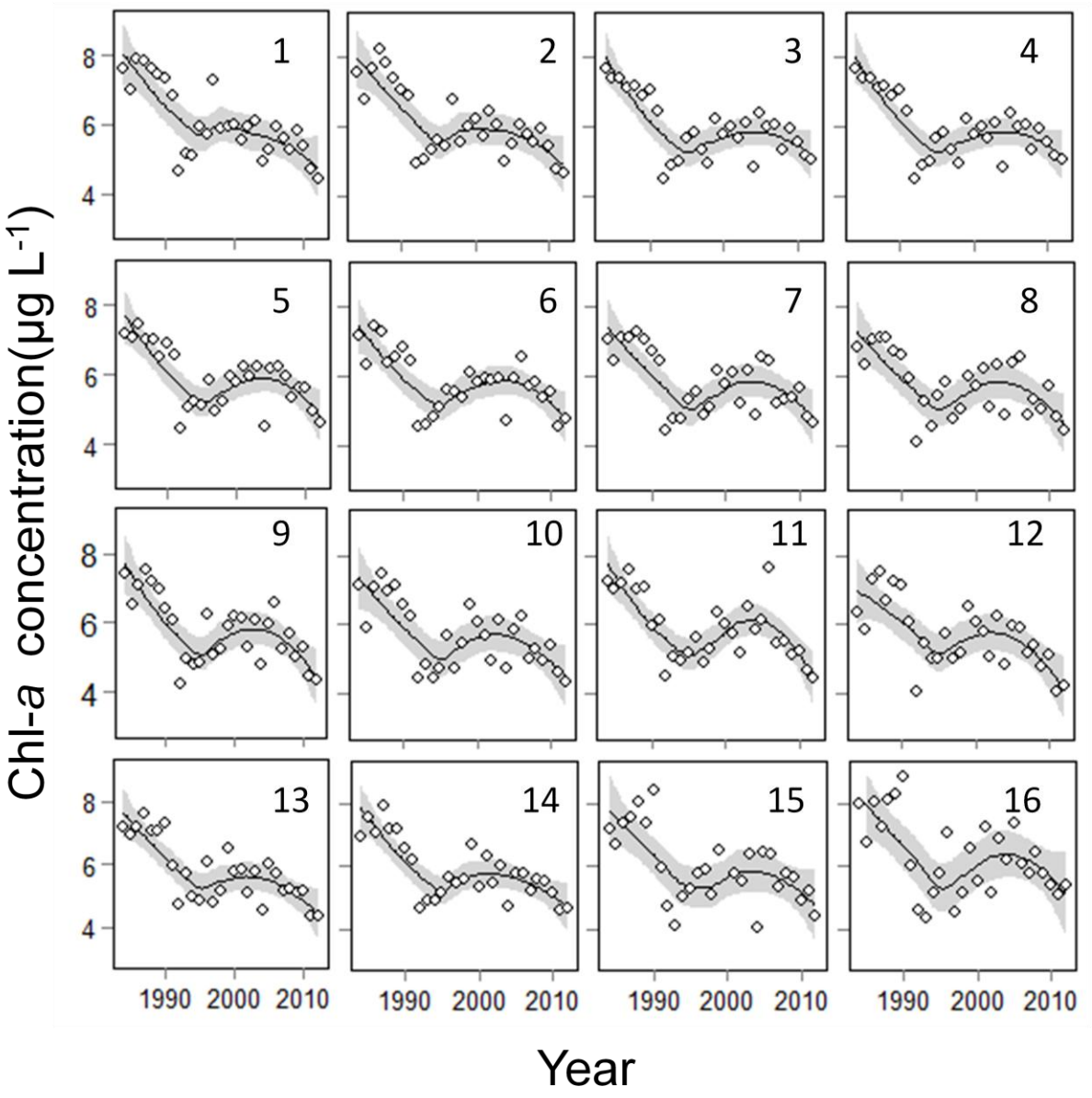

Fig. 3.9. Relationship between Chl-*a* and year at each site. Chlorophyll-*a* declined with a sigmoidal pattern between 1984-2012 at all sites. Each relationship is fitted to a LOESS smoothed line, and the gray areas represent 95% confidence intervals. Site numbers are arranged such that low numbers are close to the reservoir inflow, and high numbers are near the outflow. A single point in each panel represents a monthly mean from a single year.

3.3.5 Spatial and Temporal Patterns in Algal Blooms

I detected algal blooms in 12 of 136 images (~9%). There were several years where algal blooms were not observed. One year (1999) had two image dates with large algal blooms. The majority of the algal blooms were found in to the Qu'Appelle arm of the reservoir (Fig. 3.10).

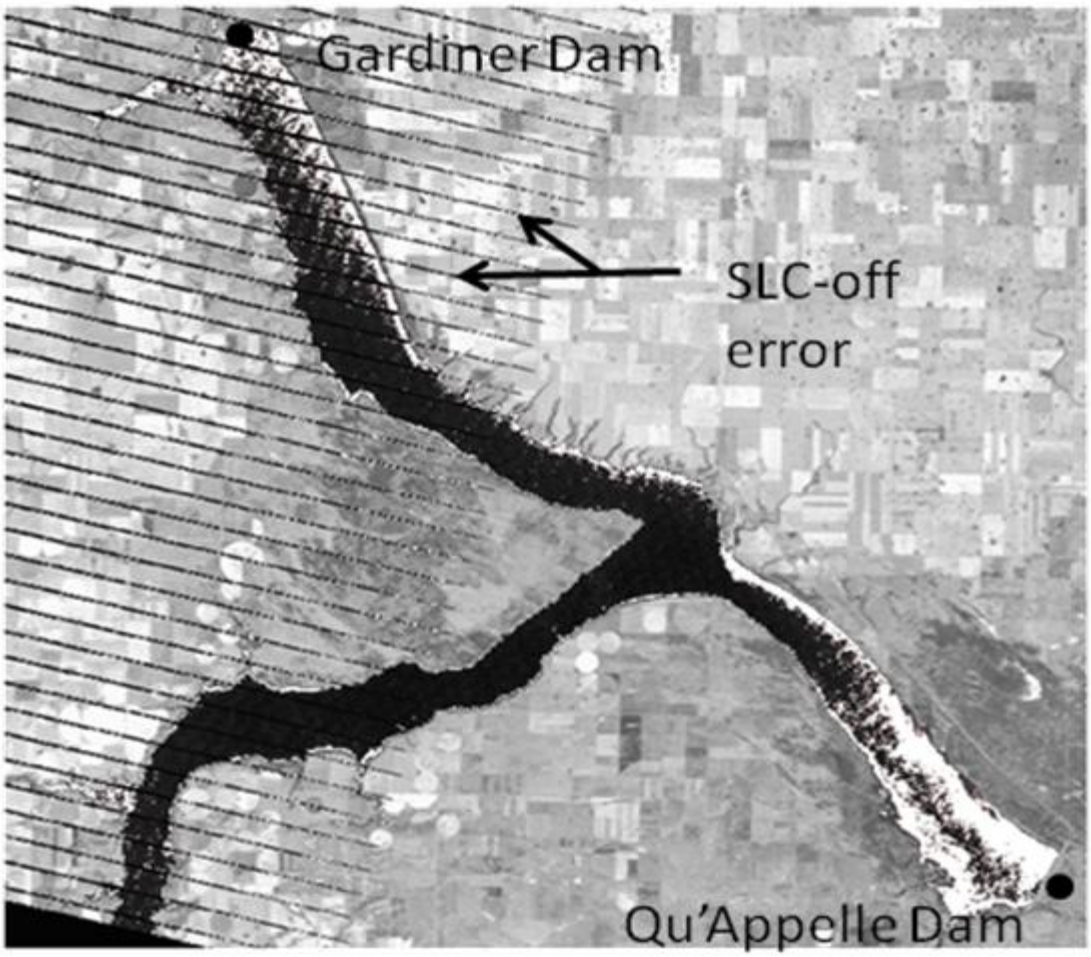

Fig. 3.10. Algal blooms in the Qu'Appelle and Gardiner arms of the reservoir. The majority of blooms had activity in these portions of the reservoir This bloom took place in October of 2006. White colored areas indicate areas that are undergoing algal blooms. Chlorophyll-*a* concentration is greater than 8 μg L^{-1} in these areas. Recurring lines indicate data loss caused by the SLC failure in 2003 aboard Landsat 7.

Only two images had blooms that covered multiple regions of the reservoir. Bloom activity was most frequently observed between August and October when wind speeds were

low (Table 3.1). Typically, Chl-*a* concentrations exceeded 8-10 µg L^{-1} in algal blooms and were characterized by rapid increases in band 3 reflectance and decreases in band 4 reflectance.

Table 3.1. Algal blooms that were imaged during the study period. The location column delineates where blooms were found. QA = Qu'Appelle Arm, GA = Gardiner arm. Wind speed refers to the average wind speed at the time in kilometers per hour (kph) the image was acquired. Wind speed was unavailable for Oct 23rd, 1995.

Date	Location	Wind Speed (kph)
Oct 8th, 1984	QA Only	15
Oct 2nd, 1985	QA Only	21
Sep 4th, 1989	QA Only	15
Oct 23rd, 1995	QA and GA	N/A
Aug 29th, 1999	Reservoir-wide	9
Oct 25th, 1999	QA and GA	7
Oct 5th, 2003	QA Only	7
Oct 10th, 2005	QA Only	15
Oct 5th, 2006	QA Only	8
Sept 14th, 2007	QA and GA	19
Oct 2nd, 2008	QA Only	11
Sep 25th, 2011	QA and GA	2

3.4 Discussion

3.4.1 Model Performance and Water Quality Relationships

I tested the accuracy of the predictive SDD and Chl-*a* models by comparing them to pre-existing data that was not used in the development of these models. The RMSE values for both SDD and Chl-*a* were comparable to other similar studies (McCullough et al. 2012;Giardino et al. 2001; Brivio et al. 2001). In addition, my models were developed from multiple samples, dates, images, and lake conditions, making them applicable to almost any Landsat image.

The positive relationship between SDD and Chl-*a* concentration is atypical for lakes as algal turbidity usually causes a decrease in water clarity (Carlson 1977), However, this result is often found in reservoirs during high flow events. Lake Diefenbaker has had multiple high flow events during my study period; most recently in 2011 and 2012 (Hudson and Vandergucht, unpublished manuscript). High flows can transport sediment and debris and create turbid conditions in many reservoirs (Cesare et al. 2001). In turn, this can cause light limitation which will suppress algal growth. Sobolev et al. (2009) noticed this pattern in highly turbid conditions in a Mississippi reservoir and Lind (1986) found the same in some Texas reservoirs. Lind also noticed the absence of a relationship between Chl-*a* concentration and SDD in most reservoirs. Canfield and Bachmann (1981) also found that the typical relationship between SDD and Chl-*a* concentration is less applicable in artificial water bodies (such as reservoirs), due in part to non-algal turbidity. However, Diefenbaker has a relatively low Chl-*a* concentration range, and the turbidity effects that occur early in the year may be the primary driver of the positive relationship. It is possible that if the reservoir had higher nutrients, a more typical Chl-*a* and water clarity relationship might emerge.

3.4.2 Flow Rate and Water Quality Variables

High flows that occur in the spring and summer are a major event on Lake Diefenbaker (Hudson and Vandergucht. unpublished manuscript; Vogt et al., accepted manuscript). High flows bring sediment that enters the reservoir and creates turbidity, which both can be important factors in reservoir behavior (Thornton et al. 1990). Data from 2013 showed that turbidity rapidly increases (from <10 NTU to >200 NTU) when these flows occur (Hudson and Vandergucht. unpublished manuscript). As such, I investigated how flow affected SDD and Chl-

a patterns. Historical flows from the SSR (station 05AJ001) and the Red Deer River (station 05CK004) were acquired and combined (www.wsc.ec.gc.ca/applications/H2O/index-eng.cfm). Flow was adjusted to account for the time it takes for water to reach the reservoir from these upstream measuring stations. Mean seasonal (May-October), mean yearly flows, and peak yearly flows were acquired from these stations, and compared to water quality variables by regression analysis (model II).

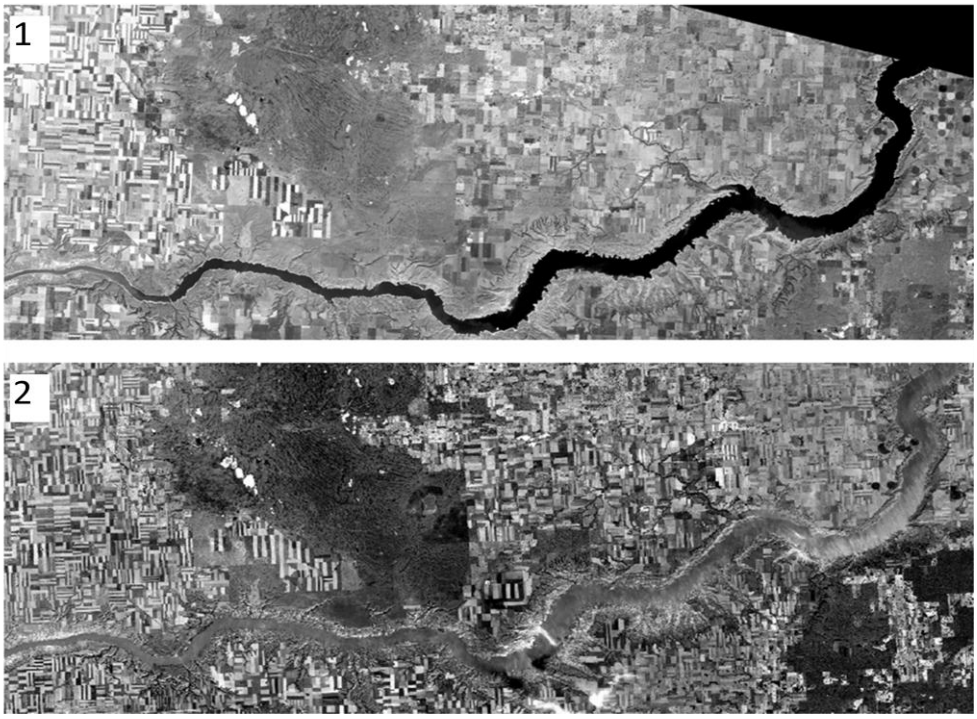

Fig. 3.11. High flow effects on water clarity in LD. Panel 1 shows the appearance of water during a low flow year, while Panel 2 shows the water during a high flow. Not only do these high flows change the appearance of the water, but it also causes decreases in water clarity. These two images are taken on the same date from two different years (Panel 1 – June 29th, 2000; Panel 2 – June 29th, 2011).

Mean yearly (Jan-Dec) and mean seasonal flow volume (May-October) had a negative linear relationship with seasonal mean SDD and Chl-*a* concentration. In other words, as flow volume increased, both water clarity and Chl-*a* concentration decreased. Relationships between flow and water quality were strongest when average seasonal flows (n=29, *p*=0.021,

R^2=0.25 for Chl-*a* and, *p*=0.048, R^2=0.28 for SDD) were used. Mean annual flows also had a significant relationship (n=29, *p*=0.044, R^2=0.15 for Chl-*a* and *p*=0.046, R^2= 0.23 for SDD). This indicates that high flows have a relatively short-term effect on SDD and Chl-*a* concentration. Peak flow did not have any significant relationship with water quality however, indicating flows must be consistently high in a season to affect water quality.

The flow of the SSR basin has actually decreased during the past century (Schindler and Donahue 2006), but in the 29 year period examined in my study, flow volume into Lake Diefenbaker has slightly increased both seasonally and annually. A number of studies have showed that snowmelt in the Rocky Mountains has begun several days earlier in the last century (Rood et al. 2008; Stewart et al. 2004). In addition, rising temperatures may cause greater peak flows in spring and summer follower by a drought period during the rest of the year (van Katwijk et al. 1993). This in turn might also lead to a greater frequency of high flow and turbidity events in the reservoir. As a result, the water quality trends identified in LD are unpredictable, and will continue to change in the future as climate change progresses (Arrigoni et al. 2010; Pomeroy et al. 2009).

The regime shifts in SDD and Chl-*a* corresponded with years that experienced abnormally high flows. The surge of melt water that arrives in June brings sediment, debris, and nutrients into LD. A large portion of this sediment became suspended in the water column and travels down the length of the LD, typical of other reservoirs (Mouri et al. 2011). Godlewska et al (2003) showed that Chl-*a* can actually decrease during high flow events, despite the added input of nutrients. Because the euphotic zone is very shallow during this time (Abirhire et al. unpublished manuscript), algal receive minimal sunlight and algal production is suppressed.

Once high flows subside, turbidity decreases as it encounters lower velocity water and light limitation becomes less prevalent in the reservoir (Abirhire et al. unpublished manuscript).

3.4.3 Trends in Reservoir SDD and Chl-a Concentrations within a Single Year

Temporal Trends: Single Year

Based on my measurements of SDD and Chl-*a* concentration, LD is a mesotrophic or mildly eutrophic reservoir (Carlson 1977). SDD underwent a predictable seasonal cycle at LD (Fig. 3.4 panel 1). Early in May, SDD was moderately deep (mean of 4.3m). A slight reduction in SDD during this time occurs likely as a result of water level increase, local melting, precipitation, and water column mixing. Ashmore and Day (1988) found that the eastern portions (including LD) of the South Saskatchewan River Basin (SSRB) experience a marked decrease in water clarity in late April and early May due to the local snowmelt. When high flows arrive in the reservoir (late May and June), increased turbidity further reduced SDD (mean of 3.7m). Some of this turbidity settled to the bottom of the reservoir, while some is flushed downstream of the reservoir in July and the rest of the season. This caused an increase in SDD throughout the remaining part of the season. SDD was typically deepest in October (5m mean). Nellis et al. (1998) found similar seasonal results in Tuttle Reservoir, Kansas, where high levels of precipitation and inflow into the reservoir caused decreases in water clarity until late July.

The average yearly Chl-*a* concentration minimum is May or June (5.4 $\mu g\ L^{-1}$ mean). Chl-*a* concentration then increased steadily throughout the year, reaching a maximum in September and October (6.9 $\mu g\ L^{-1}$ mean; Fig. 3.4, panel 2). Algal blooms were typically found in September or October. This pattern is typical in temperate lakes with relatively low mean Chl-*a* concentrations (Marshall and Peters 1989).

Spatial Trends: Single Year

Secchi disk depth underwent a predictable spatial cycle each year. Water clarity was consistently lower near the inflow, especially during years with high flow (Fig. 3.4, panel 1). Upstream sites had continually lower water clarity because of continued flows throughout the season. Downstream sites typically only exhibited reductions in water clarity during times of high flow. These downstream sites have relatively deep Secchi depths during the remainder of the season because much of the sediment that entered earlier from the SSR has settled to the bottom of the reservoir or has been flushed.

For any period of time, Chl-*a* concentrations varied by 1-2 $\mu g\ L^{-1}$ along the length of the reservoir (Fig. 3.7). The Qu'Appelle arm of the reservoir was an exception and Chl-*a* concentrations tended to be slightly greater. This location had the greatest occurrence of by fall algal blooms, potentially explaining this trend.

3.4.4 Historical Trends in Water Quality Variables (1984 - 2012)

Temporal Trends in Water Quality from 1984 to 2012

A non-linear pattern was observed in the long-term water quality patterns that were predicted from the archived satellite imagery. The regime shift analysis (RSA) isolated two major declining shifts in SDD and Chl-*a* in 1992 and 2011. I believe these reductions in water clarity and Chl-*a* concentration are likely a result of the increased turbidity brought by high flows discussed in the previous section. All months studied had net decreases in SDD and Chl-*a* concentration from 1984-2012 except October (Fig. 3.5 and Fig. 3.6, lower panels). Each month had a decline in the mean SDD and Chl-*a* concentration from its initial value in 1984, but the rates and magnitude of decline were not identical in every month. July Chl-*a* concentration has

remained relatively constant. The Chl-*a* concentration in October has decreased from its initial 1984 concentration, but started to increase from the middle of the 1990s. Algal blooms occurred most frequently in October, possibly explaining why algal concentrations were highest here. These patterns in October are likely related; higher water clarity decreases light limitation and leads to higher algal concentrations.

Spatial Changes in Water Quality from 1984-2012

The pattern in SDD was similar in shape across sites, but varied in magnitude depending on site proximity to SSR (Fig. 3.8). Again, this is likely caused by the high flows that enter the reservoir during spring and summer. The greatest turbidity enters in the upstream portions, and gradually settles out of the water column as water flows down the reservoir (Hudson and Vandergucht, unpublished manuscript). This behavior is likely related to the morphometry of reservoirs in general (Callender and Metre 1997; Kennedy and Walker 1990). Despite the obvious differences in water clarity, the pattern of decline in Chl-*a* concentration appears similar at all sites in both magnitude and shape (Fig. 3.9). Hecker et al. (2012) also noticed this pattern in a single year. We theorize then, that light limitation caused by high flows may be limiting algal growth throughout the reservoir during the spring and early summer, but it settles quickly and algal production increases later in the summer and fall.

3.4.5 Algal Bloom Timing and Frequency

My review of archived satellite imagery indicates that algal blooms were not a recent development at LD. Algal blooms were first detected in the first year of my study (1984). There is also evidence which suggests that algal blooms occurred in LD and the Qu'Appelle river lakes before satellite imagery was available (Hammer 1971). However, algal blooms were not

consistent in timing or distribution. This suggests that LD does not consistently have the conditions necessary for algal blooms. The appearance of algal blooms is likely governed by external (e.g., flow, meteorology) as well as internal reservoir conditions (e.g., nutrient concentrations; Michalak et al. 2013). However, when algal blooms did occur they were observed primarily in the late summer and fall. This period corresponds with peak annual water temperatures. High water temperatures promote algal growth (especially cyanobacteria) compared to cooler waters present earlier in the year (Johnk et al. 2008; Paul 2008). Calm weather is also shown to promote algal bloom formation by allowing buoyant algae to rise to the surface (Reynolds and Walsby 1975; Kanoshina et al. 2003). Cyanobacterial blooms often form during this time because of their ability to control their buoyancy (Walsby 1994). In addition, there is evidence that blooms in Lake Diefenbaker often consist of *Anabaena* spp and other blue green algae (Abirhire et al. unpublished data; Hecker et al. 2012). During strong winds algae are mixed within the water column, but during calm water periods, algae can rise and accumulate near the surface. Wind speed minimums of 21-28 kilometers per hour (km h^{-1}) are necessary to homogenize water columns and disperse algal blooms back down (Kahru et al. 1993). In fact, the majority of blooms that were captured in satellite images occurred when wind speeds were below this threshold (Table 3.1). Large blooms on August 9th, 1990 and September 25th, 2011 were exposed to winds of only nine km h^{-1} and four km h^{-1} respectively (http://climate.weather.gc.ca/index_e.html). This means that algal blooms can appear and disappear quickly if wind conditions change rapidly. Therefore, to best predict the onset and maintenance of algal blooms, a variety of factors must be monitored (e.g., nutrient and meteorological conditions).

3.4.6 Algal Bloom Distribution

The majority of algal blooms occurred in the Qu'Appelle arm of the reservoir. There are several possible explanations for the localization of algal blooming in this area. This part of the reservoir is isolated from the primary flow path, which flows towards the Gardiner dam. As a result, the Qu'Appelle arm has a residence time of approximately 26 years compared to a residence time of 2.5 years for the whole reservoir (Costa 2011). Longer residence times are more conducive to algal bloom formation (Hudnell 2010; Paerl et al. 2008; Søballe and Kimmel 1987). The Qu'Appelle arm of the reservoir is also considerably shallower than a large portion of the reservoir, meaning nutrient resuspension may be greater here as well. The Qu'Appelle and Gardiner arms may also experience a lesser degree of light limitation caused by non-algal turbidity compared to upstream regions. These areas of the reservoir undergo a smaller reduction in water clarity during high and low flows (Fig. 3.8 and Fig. 3.11). As a result of the above factors in this section and section 3.4.5 (high seasonal water temperature, stagnant water, light availability, nutrient availability), it would appear that the Qu'Appelle arm in the fall has the highest likelihood of experiencing algal blooms (Paerl and Huisman 2008; Paerl, 2008).

3.4.7 Satellite Monitoring Limitations

Algal blooms had to be 15m in size before they were detectable on the satellite imagery. Therefore, small or very patchy blooms may be overlooked because of the limited spatial resolution of the Landsat satellites. However, these small blooms likely were not significantly affect water quality. The temporal resolution of the satellites likely led to the underreporting of algal blooms throughout the study as well. My satellite models are incapable of detecting most subsurface algal blooms because reflected light is minimal from deep waters and often difficult

to isolate, making identification of subsurface blooms difficult. There is evidence that many algal blooms originate in subsurface waters and later rise to the surface. As such, these blooms may not be detected until they reach the surface, despite their impact on water quality.

3.4.8 Future Directions

Analysis of the archive Landsat 5 and 7 images has demonstrated a set of long-term patterns in SDD and Chl-*a* concentrations in the reservoir. The interaction of flow, nutrients, climate, and reservoir morphometry are interacting to influence water quality. Although I have provided some insight on the role of these variables on historical patterns, a more detailed analysis is warranted, but beyond the scope of this study. Future work should also aim to improve the strength of my models that predicted both SDD and Chl-*a* concentration. This could be done through the review of additional satellite imagery and field sampling. Most satellite models are developed with only one or two days of satellite imagery, but my study is more comprehensive. It contains data and imagery from multiple passes, seasons, and through a wider range of conditions. As a result, the explanatory power (R^2) of my models may be lower, but they have a much greater range of applicability.

The development of new models that predict other water quality variables may as help to better understand the reservoir. Logically, the next step will be to generate a model that measures turbidity. This is turn may be used to better estimate both SDD and Chl-*a* concentrations. Furthermore, models that predict additional water quality variables, such as suspended sediment or temperature, will allow me to better characterize the water quality of the reservoir

3.5 Conclusions

This study highlights a small portion of the data that the Landsat program can contribute to our knowledge of Lake Diefenbaker. The Landsat imagery here supplements our existing knowledge of the system, but also can provide background water quality data for Lake Diefenbaker. This is especially important because historical data for the reservoir has been sporadic and incomplete since the construction of the reservoir was completed. The study has acquired monthly water quality data from a lengthy and continuous archive that dates back to 1984. We conclude that although water clarity has decreased, and surface chlorophyll concentrations have decreased, additional monitoring is necessary to determine if these changes are permanent or part of a cycle the reservoir experiences. We also conclude that algal blooms are an occasional event on Lake Diefenbaker, but there is not enough evidence to suggest that they are becoming problematic.

Chapter 4 – Thesis Summary and General Conclusions

A foundation of baseline knowledge about the current and historical state of a water body is essential for proper management. However, this level of knowledge is lacking for many ecosystems. Data acquired from historical satellite imagery can help to fill this gap of knowledge. The relatively low cost and the ability for satellites to image a large area makes remote sensing an ideal option for studying remote systems or engaging in long-term monitoring programs. Multiple studies have shown that the Landsat satellites can be utilized for water quality monitoring. Fewer studies, however, are focused on studying reservoirs and their unique characteristics. My study had several accomplishments, which can be condensed into the following:

1. I developed models that can predict Secchi disk depth and chlorophyll-*a* concentration at LD using Landsat imagery.
2. I determined the effects of a time lag between image acquisition and field data collection, and I determined how accurately the models could predict SDD and Chl-*a*.
3. I investigated long-term trends in the SDD and Chl-*a* concentration and their causes using an imagery archive that extends from 1984-2012.
4. I analyzed the effects of short term events, such as high flow events and algal blooms on the reservoir's SDD and Chl-*a* concentration.

Field-acquired water quality measurements (Chl-*a* concentration and SDD) from LD, along with Landsat imagery of the reservoir were acquired from the USGS in 2011 and 2012. I developed novel models that were able to predict the Chl-*a* concentration and SDD in the

reservoir using this data (Chapter 2.3.3). The models explained slightly less variation than models used in comparable studies, but were more versatile as they could be applied to any good quality Landsat 5 or 7 images. This is because they were developed from two seasons of sampling, instead of a small number of images. The models that were developed feature band combinations that are capable of detecting and accounting for the high turbidity that occurs in the spring and early summer at LD. The SDD model was shown to be more accurate than the Chl-*a* model using RMSE and regression models as a basis for comparison (Chapter 2.3.6). The Chl-*a* model was also found to underestimate actual Chl-*a* values, but could still effectively identify changes in algal concentration. The model could also identify the presence and extent of surface algal blooms. In 2011 and 2012, the SDD and Chl-*a* models were used to investigate the yearly variation in the reservoir. However, by applying the models developed in 2011 and 2012 to the historical archive (1984-2012), I was able to examine temporal and spatial trends that have occurred in the reservoir in the past three decades.

Mean reservoir Chl-*a* concentration has decreased during the study period (Chapter 3.4.3). The decline in Chl-*a* concentration is similar is all months studied except of July and October. Spatially, the mean decrease in reservoir Chl-*a* concentration is similar from site to site. The reservoir could be considered mesotrophic to lightly eutrophic throughout the study period (Carlson 1977). Water clarity has also declined during the study period. All months studied had a decline in water clarity except October. Spatially, the reduction in water clarity was greatest near the SSR, with sites further downstream in the reservoir experiencing a progressively smaller reduction in water clarity. High flows entering LD between late May and early July significantly affects seasonal water quality (Chapter 3.4.2). These flows cause the

formation of a large turbidity plume that reduces water clarity and SDD values. This plume can also cause light limitation in the reservoir, which can contribute to low algal production. However, caution should still be taken regarding the management of nutrient input in the reservoir to ensure that it does not cross a threshold that would significantly alter its water quality.

There are several important conclusions that this study revealed about LD. First, this study was able to develop novel models that were capable of predicting water quality, despite high turbidity that the reservoir experiences during high flow events. The band combinations are unique to my study, but fulfill the same purposes as other studies. Second, the typical negative relationship between SDD and Chl-*a* concentration (e.g., Kalff 2002) is not found at LD. Instead, I found a positive relationship between predicted SDD and predicted Chl-*a*. As a result, I conclude that increases in algal concentrations are not the primary cause for reductions in water clarity at LD. Instead, there is indirect evidence that non-algal turbidity caused these reductions in water clarity. Additionally, flow rate is a significant driver of the activity in LD because increases in turbidity are associated with high flow (Hudson and Vandergucht 2014). There was a negative relationship between flow and both SDD and Chl-*a* concentration. Finally, algal blooms have occurred throughout the period of my study, but I did not find evidence that it has become a more frequent or severe event in the reservoir. As a result, I was able to conclude that the water quality of LD has not decreased as a result of increasing algal concentrations.

Much more future work can be initiated using the data and methods obtained in this study. A model which predicts turbidity would be the next step, as this could lend more direct

evidence towards the effect of a high flow event on the reservoir. Additional models, such as one that can predict surface water temperature or suspended sediment concentrations could also be developed. As an alternative, water quality variables that were not modeled in this study may be inferred by using known relationships. An example of this would be the relationship between SDD and turbidity (Brezonik 1978 and Effler 1988). This study used total Chl-*a* concentration as a proxy for algal biomass. Some algal groups that produce Chl-*a,* such as cyanobacteria, are potentially more problematic than others. It has been shown that identifying these blue-green algae based on their specific pigments is possible (Vincent et al. 2004), and future studies may be able to determine if there have been any changes in cyanobacteria behavior in the reservoir's history. It may also be useful to review additional satellite imagery to increase the explanatory power of the Chl-*a* model. It will also be useful for the imagery from this project to be distributed it to reservoir managers and interested parties. The development of an online database where interested parties could access reservoir information would be warranted. Olmanson et al. (2008) created a database for water clarity that contains thousands of lakes in Minnesota that can be easily accessed online, and this model would be useful here as well.

My study had several limitations that were imposed by the technology I used. Although the Landsat satellites have a proven history of success, they do have some weaknesses. Temporal resolution was restricted to eight days, meaning that significant short-term events (such as algal blooms) may have been overlooked. Similarly, the 30 x 30 m spatial resolution limits my ability to access data from small bays or near the shoreline. There are satellites that are better capable of imaging these smaller areas, but their operational cost was beyond the

budget of this study. There were also some environmental conditions that limited my study. First, the sampling years (2011 and 2012) had flows that were considerably above average. As such, the effects of low flow years may not have been adequately represented in the models. Second, algal blooming was only captured on a single image in my sampling years (2011 and 2012). As such, very high Chl-*a* concentrations and the reflective effects on satellite imagery caused by high algal concentrations may not have been adequately incorporated in the models.

I would recommend the following additions if I were to repeat this study. First, I would add sampling days before and after image acquisition to confirm and expand on the results from my time-window analysis. This increase in sampling frequency may improve model strength or help to determine at what length of time models no longer predict water quality precisely. Second, I would incorporate different atmospheric correction methods to determine which is best at removing the effect of atmospheric haze. Although dark-object subtraction techniques are still useful (Song et al. 2001; Chavez 1996), newer and more complex methods exist that may better represent atmospheric conditions and help improve model strength. Last, the acquisition and use of a portable high resolution radiometer could potentially improve model strength. This radiometer would be able to remove the effect of light that reflects directly off the surface of the water without interacting with the Chl-*a* or other substances in the water. In addition, a radiometer might help isolate signals given off by specific groups of algae or sediments within the water column.

Furthermore, developing multiple models for the reservoir may generate more accurate data. For example, it may be helpful to have a different set of models that predict water quality during a period of high flow. Flow volume or turbidity could be used to determine when each

model was used. The reservoir could also be split into multiple sections that each have a different model. This may be relevant because we know that certain areas of the reservoir (such as the Qu'Appelle Arm) behave differently from the rest of the reservoir. Additionally, my study used linear regression models, as many previous studies have done before. However, mixed effects models or non-linear models may explain additional variation in the models, and should be investigated in the future.

This study has showed that Landsat satellites were able to provide water quality information from Lake Diefenbaker over the past several decades. This research also highlights the need for continued monitoring, and how satellite imagery can provide this information. It is necessary to determine if the water quality trends identified in this study are unidirectional, or if they are part of a cyclical pattern in water quality at LD. The launch of Landsat 8 will be able to provide a continuous dataset for the foreseeable future. The work in this thesis allows for water quality information to be extracted at minimal cost while obtaining information for every part of the reservoir. This information will allow policy makers to obtain the data they need to make informed decisions regarding the management and future of the reservoir.

Literature Cited

Abirhire, O., Hunter, K., Prestie, C., Yip, H., Johansson, J., Sereda, J., North, R., Hudson, J. Environmental foctors influencing phytoplankton in Lake Diefenbaker, SK, Canada. Unpublished Manuscript. 2014.

Allan, M.G., Hamilton, D.P., Hicks, B.J., Brabyn, L., 2011. Landsat remote sensing of chlorophyll a concentrations in central North Island lakes of New Zealand. International Journal of Remote Sensing 32, 2037–2055.

Allee, R.J., Johnson, J.E., 1999. Use of satellite imagery to estimate surface chlorophyll a and Secchi disc depth of Bull Shoals Reservoir, Arkansas, USA. International Journal of Remote Sensing 20, 1057–1072.

Anderson, D.M., Glibert, P.M., Burkholder, J.M., 2002. Harmful algal blooms and eutrophication: Nutrient sources, composition, and consequences. Estuaries 25, 704–726.

Andréfouët, S., Berkelmans, R., Odriozola, L., Done, T., Oliver, J., Müller-Karger, F., 2002. Choosing the appropriate spatial resolution for monitoring coral bleaching events using remote sensing. Coral Reefs 21, 147–154.

Arrigoni, A.S., Greenwood, M.C., and Moore, J.N., 2010. Relative impact of anthropogenic modifications versus climate change on the natural flow regimes of rivers in the Northern Rocky Mountains, United States. Water Resources, 46.

Ashmore, P.E., Day, T.J., 1988. Spatial and temporal patterns of suspended-sediment yield in the Saskatchewan River basin. Can. J. Earth Sci. 25, 1450–1463.

Baban, S.M., 1993. Detecting water quality parameters in the Norfolk Broads, UK, using Landsat imagery. International Journal of Remote Sensing 14, 1247–1267.

Barnes, B.B., Hu, C., Holekamp, K.L., Blonski, S., Spiering, B.A., Palandro, D., Lapointe, B., 2014. Use of Landsat data to track historical water quality changes in Florida Keys marine environments. Remote Sensing of Environment 140, 485–496.

Baron, J.S., Driscoll, C.T., Stoddard, J.L., Richer, E.E. 2011. Empirical Critical Loads of Atmospheric Nitrogen Deposition for Nutrient Enrichment and Acidification of Sensitive

US Lakes. Bioscience 61, 602-613

Bergmann, M., Peters, R.H., 1980. A simple reflectance method for the measurement of particulate pigment in lake water and its application to phosphorus-chlorophyll-seston relationships. Canadian Journal of Fisheries and Aquatic Sciences 37, 111–114.

Bilge, F., Yazici, B., Dogeroglu, T., Ayday, C., 2003. Statistical evaluation of remotely sensed data for water quality monitoring. International Journal of Remote Sensing 24, 5317–5326.

Bogard, M.J., Donald, D.B., Finlay, K., Leavitt, P.R., 2012. Distribution and regulation of urea in lakes of central North America. Freshwater Biology 57, 1277–1292.

Boyce, D.G., Lewis, M.R., Worm, B., 2010. Global phytoplankton decline over the past century. Nature 466, 591–596.

Boynton, W.R., Garber, J.H., Summers, R., Kemp, W.M., 1995. Inputs, transformations, and transport of nitrogen and phosphorus in Chesapeake Bay and selected tributaries. Estuaries 18, 285–314.

Brezonik, P., Menken, K.D., Bauer, M., 2005. Landsat-based remote sensing of lake water quality characteristics, including chlorophyll and colored dissolved organic matter (CDOM). Lake and Reservoir Management 21, 373–382.

Brezonik, P.L., 1978. Effect of Organic Color and Turbidity of Secchi Disk Transparency. J. Fish. Res. Bd. Can. 35, 1410–1416.

Brivio, P.A., Giardino, C., Zilioli, E., 2001. Determination of chlorophyll concentration changes in Lake Garda using an image-based radiative transfer code for Landsat TM images. International Journal of Remote Sensing 22, 487–502.

Bustamante, J., Pacios, F., Díaz-Delgado, R., Aragonés, D., 2009. Predictive models of turbidity and water depth in the Doñana marshes using Landsat TM and ETM+ images. Journal of Environmental Management 90, 2219–2225.

Callender, E., Metre, P.C.V., 1997. Environmental policy analysis, peer reviewed: reservoir sediment cores show US lead declines. Environmental science & technology 31, 424A–428A.

Canfield Jr, D.E., Brown, C.D., Bachmann, R.W., Hoyer, M.V., 2002. Volunteer lake monitoring: testing the reliability of data collected by the Florida LAKEWATCH program. Lake and Reservoir Management 18, 1–9.

Canfield Jr., D.E., Bachmann, R.W., 1981. Prediction of Total Phosphorus Concentrations, Chlorophyll a, and Secchi Depths in Natural and Artificial Lakes. Can. J. Fish. Aquat. Sci. 38, 414–423.

Carder, K.L., Chen, F.R., Cannizzaro, J.P., Campbell, J.W., Mitchell, B.G., 2004. Performance of the MODIS semi-analytical ocean color algorithm for chlorophyll-a. Advances in Space Research, Climate Change Processes in the Stratosphere, Earth-Atmosphere-Ocean Systems, and Oceanographic Processes from Satellite Data 33, 1152–1159.

Carlson, R.E., 1977. A Trophic State Index for Lakes. Limnology and Oceanography 22, 361–369.

Carmichael, W.W., 2001. Health effects of toxin-producing cyanobacteria: "The CyanoHABs". Hum. Ecol. Risk Assess. 7, 1393–1407.

Carpenter, D.J., Carpenter, S.M., 1983. Modeling inland water quality using Landsat data. Remote Sensing of Environment 13, 345–352.

Carpenter, S.R., Caraco, N.F., Correll, D.L., Howarth, R.W., Sharpley, A.N., Smith, V.H., 1998. Nonpoint pollution of surface waters with phosphorus and nitrogen. Ecol. Appl. 8, 559–568.

Cesare, G., Schleiss, A., Hermann, F., 2001. Impact of Turbidity Currents on Reservoir Sedimentation. Journal of Hydraulic Engineering 127, 6–16.

Chander, G., Markham, B.L., Helder, D.L., 2009. Summary of current radiometric calibration coefficients for Landsat MSS, TM, ETM+, and EO-1 ALI sensors. Remote Sensing of Environment 113, 893–903.

Chavez Jr, P.S., 1988. An improved dark-object subtraction technique for atmospheric scattering correction of multispectral data. Remote sensing of Environment 24, 459–479.

Chavez, P.S., 1996. Image-based atmospheric corrections-revisited and improved. Photogrammetric engineering and remote sensing 62, 1025–1035.

Chen, J., Fu, J., Zhang, M., 2011. An Atmospheric Correction Algorithm for Landsat/TM Imagery Basing on Inverse Distance Spatial Interpolation Algorithm: A Case Study in Taihu Lake. IEEE Journal of Selected Topics in Applied Earth Observations and Remote Sensing 4, 882–889.

Chipman, J.W., Lillesand, T.M., Schmaltz, J.E., Leale, J.E., Nordheim, M.J., 2004. Mapping lake water clarity with Landsat images in Wisconsin, U.S.A. Canadian Journal of Remote Sensing 30, 1–7.

Costa, D., 2011. Eutrophication of Lake Diefenbaker (MSc Thesis). Imperial College, London, England.

Crétaux. J.F., Jelinski, W., Calmant, S., Kouraev, A., Vuglinski, V. Bergé-Nguyen, M. Gennero, M.C., Nino, F., Del Rio, R.A., Cazenave, A. Maisongrande P. 2011. SOLS: a lake database to monitor in the Near Real Time water level and storage variations from remote sensing data. Advances in Space Research 47, 1497-1507.

Darecki, M., Stramski, D., 2004. An evaluation of MODIS and SeaWiFS bio-optical algorithms in the Baltic Sea. Remote Sensing of Environment 89, 326–350.

Diaz, J.C.F., Carter, W.E., Shrestha, R.L., Glennie, G.L. 2013. Lidar Remote Sensing. Handbook of Remote Sensing. 757-808

Dillon, P.J., Rigler, F.H., 1974. The phosphorus-chlorophyll relationship in lakes. Limnol. Oceanogr 19, 767–773.

Dodds, W.K., Bouska, W.W., Eitzmann, J.L., Pilger, T.J., Pitts, K.L., Riley, A.J., Schloesser, J.T., Thornbrugh, D.J., 2008. Eutrophication of US freshwaters: analysis of potential economic damages. Environmental Science & Technology 43, 12–19.

Duan, H., Ma, R., Xu, X., Kong, F., Zhang, S., Kong, W., Hao, J., Shang, L., 2009. Two-decade reconstruction of algal blooms in China's Lake Taihu. Environmental Science & Technology 43, 3522–3528.

Duan, H., Zhang, Y., Zhang, B., Song, K., Wang, Z., Liu, D., Li, F., 2008. Estimation of chlorophyll-a concentration and trophic states for inland lakes in Northeast China from Landsat TM data and field spectral measurements. International Journal of Remote Sensing 29, 767–786.

Duane Nellis, M., Harrington Jr., J.A., Wu, J., 1998. Remote sensing of temporal and spatial variations in pool size, suspended sediment, turbidity, and Secchi depth in Tuttle Creek Reservoir, Kansas: 1993. Geomorphology 21, 281–293.

Dyson, K., Huppert, D.D. 2010. Regional economic impacts of razor clam beach closures due to harmful algal blooms (HABs) on the Pacific coast of Washington. Harmful Algae 9. 264-271

Effler, S., 1988. Secchi Disc Transparency and Turbidity. Journal of Environmental Engineering 114, 1436–1447.

Effler, S.W., Matthews, D.A., Kaser, J.W., Prestigiacomo, A.R., and Smith, D.G., 2006. Runoff Event Impacts on a Water Supply Reservoir: Suspended Sediment Loading, Turbid Plume Behavior, and Sediment Deposition. *Journal of the American Water Resources Association*. 42, 16997-1710.

Espie, R.H., James, P.C., Brigham, R.M., 1998. The effects of flooding on piping plover Charadrius melodus reproductive success at Lake Diefenbaker, Saskatchewan, Canada. Biological Conservation 86, 215–222.

Giardino, C., Pepe, M., Brivio, P.A., Ghezzi, P., Zilioli, E., 2001. Detecting chlorophyll, Secchi disk depth and surface temperature in a sub-alpine lake using Landsat imagery. Science of The Total Environment 268, 19–29.

Glibert, P.M., Hinkle, D.C., Sturgis, B., Jesien, R.V., 2013. Eutrophication of a Maryland/Virginia Coastal Lagoon: a Tipping Point, Ecosystem Changes, and Potential Causes. Estuaries and Coasts 1–19.

Gober, P., Wheater, H.S. 2014. Socio-hydrology and the science-policy interface: a case study of the Saskatchewan River basin. Hydrology and Earth System Sciences 18, 1413-1422.

Godlewska, M., Mazurkiewicz-Boroń, G., Pociecha, A., Wilk-Woźniak, E., Jelonek, M., 2003. Effects of flood on the functioning of the Dobczyce reservoir ecosystem. Hydrobiologia 504, 305–313.

Gurlin, D., Gitelson, A., Moses, W., 2011. Remote estimation of Chl-a concentration in turbid productive waters - Return to a simple two-band NIR-red model? Remote Sensing of Environment. 115, 3479-3490

Hakvoort, H., de Haan, J., Jordans, R., Vos, R., Peters, S., Rijkeboer, M., 2002. Towards airborne remote sensing of water quality in The Netherlands—validation and error analysis. ISPRS Journal of Photogrammetry and Remote Sensing 57, 171–183.

Hammer, U.T., 1971. Limnological studies of the lakes and streams of the upper qu'appelle river system, Saskatchewan, Canada. Hydrobiologia 37, 473–507.

Harrington, J., Schiebe, F., Nix, J., 1992. Remote-Sensing of Lake Chicot, Arkansas - Monitoring Suspended Sediments, Turbidity, and Secchi Depth with Landsat Mss Data. Remote Sens. Environ. 39, 15–27.

Hecker, M., Khim, J.S., Giesy, J.P., Li, S.-Q., Ryu, J.-H., 2012. Seasonal dynamics of nutrient loading and chlorophyll A in a northern prairies reservoir, Saskatchewan, Canada. Journal of Water Resource and Protection 4, 180–202.

Hudnell, H.K., 2010. The state of US freshwater harmful algal blooms assessments, policy and legislation. Toxicon 55, 1024–1034.

Hudson, J., Vandergucht, D. 2014. Spatial and Temporal Patterns in Physical Properties and Dissolved Oxygen in Lake Diefenbaker, a Large Reservoir on the Canadian Prairies. Submitted Manuscript

Jarvie, H.P., Neal, C., Withers, P.J.A., 2006. Sewage-effluent phosphorus: A greater risk to river eutrophication than agricultural phosphorus? Science of The Total Environment 360, 246–253.

Jassby, A.D., Reuter, J.E., Axler, R.P., Goldman, C.R., Hackley, S.H., 1994. Atmospheric deposition of nitrogen and phosphorus in the annual nutrient load of Lake Tahoe (California-Nevada). Water Resources Research 30, 2207–2216.

Johnk, K.D., Huisman, J., Sharples, J., Sommeijer, B., Visser, P.M., Stroom, J.M., 2008. Summer heatwaves promote blooms of harmful cyanobacteria. Glob. Change Biol. 14, 495–512.

Kahru, M., Horstmann, U., Rud, O., 1994. Satellite Detection of Increased Cyanobacteria Blooms in the Baltic Sea: Natural Fluctuation or Ecosystem Change? Ambio 23, 469–472.

Kahru, M., Lepppaenen, J.-M., Rud, O., 1993. Cyanobacterial blooms heating of the sea surface. Marine ecology progress series. Oldendorf 101, 1–7.

Kalff, J. 2002. Limnology: inland water ecosystems. Prentice-Hall, Upper Saddle River, New Jersey

Kangur, K., Kangur, A., Kangur, P., Laugaste, R., 2005. Fish kill in Lake Peipsi in summer 2002 as a synergistic effect of cyanobacterial bloom, high temperature and low water level. In: Proceedings of the Estonian Academy of Sciences. Biology Ecology. pp. 67–80.

Kanoshina, I., Lips, U., Leppänen, J.-M., 2003. The influence of weather conditions (temperature and wind) on cyanobacterial bloom development in the Gulf of Finland (Baltic Sea). Harmful Algae 2, 29–41.

Karakaya, N., Evrendilek, F., Aslan, G., Gungor, K., Karakas, D., 2011. Monitoring of lake water quality along with trophic gradient using landsat data. International Journal of Environmental Science and Technology 8, 817–822.

Keeling, C., Whorf, T., Wahlen, M., Vanderplicht, J., 1995. Interannual Extremes in the Rate of Rise of Atmospheric Carbon-Dioxide Since 1980. Nature 375, 666–670.

Kennedy, R.H., Walker, W.W., 1990. Reservoir nutrient dynamics. Reservoir limnology: Ecological perspective. Wiley.

Søballe, D.M., and Kimmel, B.L.,1987. A Large-Scale Comparison of Factors Influencing Phytoplankton Abundance in Rivers, Lakes, and Impoundments. *Ecology* 68. 1943-1954.

Kloiber, S.M., Brezonik, P.L., Bauer, M.E., 2002. Application of Landsat imagery to regional-scale assessments of lake clarity. Water Research 36, 4330–4340.

Kloiber, S.N., Brezonik, P.L., Olmanson, L.G., Bauer, M.E., 2002. A procedure for regional lake water clarity assessment using Landsat multispectral data. Remote Sens. Environ. 82, 38–47.

Kutser, T., 2012. The possibility of using the Landsat image archive for monitoring long time trends in coloured dissolved organic matter concentration in lake waters. Remote Sensing of Environment 123, 334–338.

Kutser, T., Metsamaa, L., Strombeck, N., Vahtmae, E., 2006. Monitoring cyanobacterial blooms by satellite remote sensing. Estuar. Coast. Shelf Sci. 67, 303–312.

Landsberg, J.H., 2002. The effects of harmful algal blooms on aquatic organisms. Rev. Fish. Sci. 10, 113–390.

LeComte, D., 2012. International Weather Highlights 2011: Flood and Famine. Weatherwise 65, 28–33.

Likens, G.E., Bormann, F.H., 1974. Acid rain: a serious regional environmental problem. Science 184, 1176–1179.

Lind, O.T., 1986. The effect of non-algal turbidity on the relationship of Secchi depth to chlorophyll a. Hydrobiologia 140, 27–35.

Loperfido, J.V., Beyer, P., Just, C.L, Schnoor, J.L. 2010. Uses and Biases of Volunteer Water Quality Data. Environmental Science and Technology 44, 7193-7199.

Lovett, G.M., Burns, D.A., Driscoll, C.T., Jenkins, J.C., Mitchell, M.J., Rustad, L., Shanley, J.B., Likens, G.E., Haeuber, R., 2007. Who needs environmental monitoring? Frontiers in Ecology and the Environment 5, 253–260.

Magnuson, J.J., 1990. Long-term ecological research and the invisible present. BioScience 40, 495–501.

Malmqvist, B., Rundle, S., 2002. Threats to the running water ecosystems of the world. Environmental conservation 29, 134–153.

Markham, B.L., Storey, J.C., Williams, D.L., Irons, J.R., 2004. Landsat sensor performance: history and current status. Geoscience and Remote Sensing, IEEE Transactions on 42, 2691–2694.

Marshall, C.T., Peters, R.H., 1989. General patterns in the seasonal development of chlorophyll a for temperate lakes. Limnology and Oceanography 34, 856–867.

McCullough, I.M., Loftin, C.S., Sader, S.A., 2012. Combining lake and watershed characteristics with Landsat TM data for remote estimation of regional lake clarity. Remote Sensing of Environment 123, 109–115.

McCullough, I.M., Loftin C.S., Sader S.A. 2013. Lakes without Landsat? An alternative approach to remote lake monitoring with MODIS 250 m imagery. Lake and Reservoir Management 29, 89-98

McLeod, C., Hildebrand, L., Radford, D., 1999. A synopsis of lake sturgeon management in Alberta, Canada. Journal of Applied Ichthyology 15, 173–179.

Mez, K., Beattie, K., Codd, G., Hanselmann, K., Hauser, B., Naegeli, H., Preisig, H., 1997. Identification of a microcystin in benthic cyanobacteria linked to cattle deaths on alpine pastures in Switzerland. European Journal of Phycology 32, 111–117.

Michalak, A.M., Anderson E.J., Beletsky, D., Boland, S., Bosch, N.S., Bridgeman, T.B., Chaffin, T.B., Cho, K., Confesor, R., Daloglu, I., DePinto, J.V., Evans, M.E., Fahnestiel, G.L., He, L., Ho, J.C., Jenkins, L., Johengen T.H., Kuo, K.C., LaPorte, E., Liu, X., McWilliams, M.R., Moore, M.R., Posselt, D.J., Richards, R.P., Scavia D., Steiner, A.L., Verhamme, E., Wright, D.M., Zagorksi, M.A. 2013. Record -setting algal bloom in Lake Erie caused by agricultural and meterological trends consistent with expected future conditions. Proceedings of the National Academy of Sciences of the United States of America. 110, 6448-6452.

Mouri, G., Shiiba, M., Hori, T., Oki, T., 2011. Modeling reservoir sedimentation associated with an extreme flood and sediment flux in a mountainous granitoid catchment, Japan. Geomorphology 125, 263–270.

Mumby, P.J., Green, E.P., Clark, C.D., Edwards, A.J., 1998. Digital analysis of multispectral airborne imagery of coral reefs. Coral Reefs 17, 59–69.

Nas, B., Ekercin, S., Karabörk, H., Berktay, A., Mulla, D.J., 2010. An Application of Landsat-5TM Image Data for Water Quality Mapping in Lake Beysehir, Turkey. Water, Air, & Soil Pollution 212, 183–197.

Nelson, S.A., Soranno, P.A., Cheruvelil, K.S., Batzli, S.A., Skole, D.L., 2003. Regional assessment of lake water clarity using satellite remote sensing. Journal of Limnology 62, 27–32.

North, R.L., Barton, D., Crowe, A.S., Dillon, P.J., Dolson, R.M.L., Evans, D.O., Ginn, B.K., Håkanson, L., Hawryshyn, J., Jarjanazi, H., King, J.W., La Rose, J.K.L., Brabyn, L., Lewis, C.F.M., Liddle, G.E., Lin, Z.H., Longstaffe, F.J., Macdonald, R.A., Molot, L., Ozersky, T., Palmer, M.E., Quinlan R, Rennie, M.D., Robillard, M.D., Rode, D., Rühland, K.M., Schwalb, A., Smol, J.P., Stainsby, E., Trumpickas, J.J., Winter, J.G., Young, J.D., 2013. The state of Lake Simcoe (Ontario, Canada): the effects of multiple stressors on phosphorus and oxygen dynamics. Inland Waters 3, 51–74.

Nriagu, J.., Kemp, A.L.., Wong, H.K.., Harper, N., 1979. Sedimentary record of heavy metal pollution in Lake Erie. Geochimica et Cosmochimica Acta 43, 247–258.

O'Reilly, J.E., Maritorena, S., Mitchell, B.G., Siegel, D.A., Carder, K.L., Garver, S.A., Kahru, M., McClain, C., 1998. Ocean color chlorophyll algorithms for SeaWiFS. J. Geophys. Res.-Oceans 103, 24937–24953.

Obrecht, D.V., Milanick, M., Perkins, B.D., Ready, D., Jones, J.R., 1998. Evaluation of data generated from lake samples collected by volunteers. Lake and Reservoir Management 14, 21–27.

Olmanson, L.G., Bauer, M.E., Brezonik, P.L., 2008. A 20-year Landsat water clarity census of Minnesota's 10,000 lakes. Remote Sensing of Environment 112, 4086–4097.

Paerl, H.W., 2008. Nutrient and other environmental controls of harmful cyanobacterial blooms along the freshwater–marine continuum. In: Cyanobacterial Harmful Algal Blooms: State of the Science and Research Needs. Springer, pp. 217–237.

Paerl, H.W., Huisman, J., 2008. Blooms Like It Hot. Science 320, 57–58.

Paerl, H.W., Fulton, R.S. 3rd, Moisander, P.H., Dyble, J., 2001. Harmful freshwater algal blooms, with an emphasis on cyanobacteria. The Scientific World Journal 1.

Patoine, A., Graham, M.D., Leavitt, P.R., 2006. Spatial variation of nitrogen fixation in lakes of the northern Great Plains. Limnol. Oceanogr 51, 1665–1677.

Paul, J.V., 2008. Global warming and cyanobacterial harmful algal blooms. *Advances in Experimental Medicine and Biology* 619, 239-257.

Poff, N.L., Allan, J.D., Bain, M.B., Karr, J.R., Prestegaard, K.L., Richter, B.D., Sparks, R.E., Stromberg, J.C., 1997. The natural flow regime: A paradigm for river conservation and restoration. BioScience 47, 769–784.

Pollock, M., Carr, M., McMaster, G., Wu, K. 2014. Use of River2D to estimate habitat loss in a managed system. Submitted.

Pomeroy, J.W., Fang, X., Williams B. 2009. Impacts of Climate Change on Saskatchewan's Water Resources. Centre for Hydrology Report No. 6.

Pomeroy, J.W., De Boer, D., Martz, L.W., 2005. Hydrology and water resources of Saskatchewan. Center for Hydrology, Report 1.

Preisendorfer, R., 1986. Secchi Disk Science - Visual Optics of Natural-Waters. Limnol. Oceanogr. 31, 909–926.

Reynolds, C.S., Walsby, A.E., 1975. Water-blooms. Biological reviews 50, 437–481.

Röder, A., Udelhoven, T., Hill, J., Del Barrio, G., Tsiourlis, G., 2008. Trend analysis of Landsat-TM and-ETM+ imagery to monitor grazing impact in a rangeland ecosystem in Northern Greece. Remote Sensing of Environment 112, 2863–2875.

Rodionov, S., Overland, J.E., 2005. Application of a sequential regime shift detection method to the Bering Sea ecosystem. ICES Journal of Marine Science: Journal du Conseil 62, 328–332.

Rodionov, S.N., 2004. A sequential algorithm for testing climate regime shifts. Geophysical Research Letters 31.

Rood, S.B., Pan, J., Gill, K.M., Franks, C.G., Samuelson, G.M., Shepherd, A., 2008. Declining summer flows of Rocky Mountain rivers: Changing seasonal hydrology and probable impacts on floodplain forests. Journal of Hydrology 349, 397–410.

Rumery, C., Vennie, J.G., 1988. Wisconsin's Self-Help Lake Monitoring Program: A Review of the First Year — 1986. Lake and Reservoir Management 4, 81–86.

Russell-Smith, J., Ryan, P.G., Durieu, R., 1997. A LANDSAT MSS-Derived Fire History of Kakadu National Park, Monsoonal Northern Australial, 1980-94: Seasonal Extent, Frequency and Patchiness. Journal of Applied Ecology 34, 748–766.

Saskatchewan Environment and Public Safety (SEPS), 1988. Lake Diefenbaker and Upper South Saskatchewan River: Water quality study 1984-85. Government Report, edited by Saskatchewan Environment and Public Safety Water Quality Branch.

Saskatchewan Water Security Agency (SWSA), 2012. State of Lake Diefenbaker.

Sass, G.Z., Creed, I.F., Bayley, S.E., Devito, K.J., 2007. Understanding variation in trophic status of lakes on the Boreal Plain: A 20 year retrospective using Landsat TM imagery. Remote Sensing of Environment 109, 127–141.

Sawaya, K.E., Olmanson, L.G., Heinert, N.J., Brezonik, P.L., Bauer, M.E., 2003. Extending satellite remote sensing to local scales: land and water resource monitoring using high-resolution imagery. Remote Sensing of Environment 88, 144–156.

Schindler, D.W., 1974. Eutrophication and recovery in experimental lakes: implications for lake management. Science 184, 897–899.

Schindler, D.W., and Donahue, W.F., 2006. An impending water crisis in Canada's western prairie provinces. Proceedings of the National Academy of Sciences of the United States of America 103, 7210-7216

Schindler, D.W., Hecky, R.E., McCullough, G.K., 2012. The rapid eutrophication of Lake Winnipeg: Greening under global change. Journal of Great Lakes Research 38, Supplement 3, 6–13.

Sellner, K.G., Doucette, G.J., Kirkpatrick, G.J., 2003. Harmful algal blooms: causes, impacts and detection. J Ind Microbiol Biotechnol 30, 383–406.

Sharpe, A., Conrad, C., 2006. Community Based Ecological Monitoring in Nova Scotia: Challenges and Opportunities. Environmental Monitoring and Assessment 113, 395–409.

Singh, A., 1989. Review Article Digital change detection techniques using remotely-sensed data. International Journal of Remote Sensing 10, 989–1003.

Søballe, D.M., and Kimmel, B.L. 1987. A Large-scale Comparison of Factors Influencing Phytoplankton Abundance in Rivers, Lakes, and Impoundments. Ecology 68, 1943-1954.

Sobolev, D., Moore, K., Morris, A.L., 2009. Nutrients and Light Limitation of Phytoplankton Biomass in a Turbid Southeastern Reservoir: Implications for Water Quality. Southeastern Naturalist 8, 255–266.

Song, C., Woodcock, C.E., Seto, K.C., Lenney, M.P., Macomber, S.A., 2001. Classification and change detection using Landsat TM data: when and how to correct atmospheric effects? Remote sensing of environment 75, 230–244.

Springer, J.J., Burkholder, J.M., Glibert, P.M., Reed, R.E., 2005. Use of a real-time remote monitoring network (RTRM) and shipborne sampling to characterize a dinoflagellate bloom in the Neuse Estuary, North Carolina, USA. Harmful Algae 4, 533–551.

St. Jacques, J.-M., Sauchyn, D.J., Zhao, Y., 2010. Northern Rocky Mountain streamflow records: Global warming trends, human impacts or natural variability? Geophysical Research Letters 37, n/a–n/a.

Stewart, I.T., Cayan, D.R., Dettinger, M.D., 2004. Changes in Snowmelt Runoff Timing in Western North America under a `Business as Usual' Climate Change Scenario. Climatic Change 62, 217–232.

Straubinger-Gansberger, N., Martin, G., Kaggwa, M.N., Lawton, L., Oduor, S.O., Schagerl, M. 2014. Sudden flamingo deaths in Kenyan Rift Valley lakes. Wildlife Biology 20, 185-189.

Stumpf, R.P., Culver, M.E., Tester, P.A., Tomlinson, M., Kirkpatrick, G.J., Pederson, B.A., Truby, E., Ransibrahmanakul, V., Soracco, M., 2003. Monitoring Karenia brevis blooms in the Gulf of Mexico using satellite ocean color imagery and other data. Harmful Algae 2, 147–160.

Tanzeeba, S., and Gan, T., 2012. Potential impact of climate change on the water availability of South Saskatchewan River Basin. *Climatic Change* 112. 355-386.

Tebbs, E.J., Remedios, J.J., Harper, D.M., 2013. Remote sensing of chlorophyll-a as a measure of cyanobacterial biomass in Lake Bogoria, a hypertrophic, saline–alkaline, flamingo lake, using Landsat ETM +. Remote Sensing of Environment 135, 92–106.

Thornton, KENT W., Thornton, K. W., Kimmel, B.L., Payne, F.E., 1990. Perspectives on reservoir limnology. Reservoir limnology: ecological perspectives 1–13.

Torbick, N., Hu, F., Zhang, J., Qi, J., Zhang, H., Becker, B., 2008. Mapping Chlorophyll-a Concentrations in West Lake, China using Landsat 7 ETM+. Journal of Great Lakes Research 34, 559–565.

Tyler, A.N., Svab, E., Preston, T., Présing, M., Kovács, W.A., 2006. Remote sensing of the water quality of shallow lakes: A mixture modelling approach to quantifying phytoplankton in water characterized by high-suspended sediment. International Journal of Remote Sensing 27, 1521–1537.

Van Katwijk, V.F., Rango, A., Childress, A.E., 1993. Effect of Simulated Climate Change on Snowmelt Runoff Modeling in Selected Basins1. JAWRA Journal of the American Water Resources Association 29, 755–766.

Vincent, R.K., Qin, X., McKay, R.M.L., Miner, J., Czajkowski, K., Savino, J., Bridgeman, T., 2004. Phycocyanin detection from LANDSAT TM data for mapping cyanobacterial blooms in Lake Erie. Remote Sensing of Environment 89, 381–392.

Vogt, R.J., Sharma, S., Leavitt, P.R. Accepted manuscript (2014). Multi-decadal regulation of algal abundance and water clarity in a large continental reservoir by climatic, hydrologic, and trophic processes. Journal of Great Lakes Research.

Vörösmarty, C.J., Green, P., Salisbury, J., Lammers, R.B., 2000. Global Water Resources: Vulnerability from Climate Change and Population Growth. Science 289, 284–288.

Vörösmarty, C.J., McIntyre, P.B., Gessner, M.O., Dudgeon, D., Prusevich, A., Green, P., Glidden, S., Bunn, S.E., Sullivan, C.A., Liermann, C.R., Davies, P.M., 2010. Global threats to human water security and river biodiversity. Nature 467, 555–561.

Walsby, A.E., 1994. Gas vesicles. Microbiol Rev 58, 94–144.

Wang, Y., Xia, H., Fu, J., Sheng, G., 2004. Water quality change in reservoirs of Shenzhen, China: detection using LANDSAT/TM data. Science of the Total Environment 328, 195–206.

Westaway, R.M., Lane, S.N., Hicks, D.M., 2003. Remote survey of large-scale braided, gravel-bed rivers using digital photogrammetry and image analysis. International Journal of Remote Sensing 24, 795–815.

Woodcock, C.E., Allen, R., Anderson, M., Belward, A., Bindschadler, R., Cohen, W., Gao, F., Goward, S.N., Helder, D., Helmer, E., Nemani, R., Oreopoulos, L., Schott, J., Thenkabail, P.S., Vermote, E.F., Vogelmann, J., Wulder, M.A., Wynne, R., 2008. Free Access to Landsat Imagery. Science 320, 1011–1011.

Wulder, M.A., Masek, J.G., Cohen, W.B., Loveland, T.R., Woodcock, C.E., 2012. Opening the archive: How free data has enabled the science and monitoring promise of Landsat. Remote Sensing of Environment 122, 2–10.

Appendix A: Glossary of Terms and Acronyms

AIC - Abbreviation for Akaike Information Criterion

Algal Bloom – A rapid increase in algal biomass in an aquatic ecosystem. This increase is often accompanied by decreased water clarity, a visible surface scum, and discolored water.

Atmospheric Correction - A portion of image pre-processing that reduces or eliminates the effect of atmospheric scattering on satellite image data.

Chl-*a*- Abbreviation for Chlorophyll-*a*

ETM+ - Acronym for Enhanced Thematic Mapper Plus, a multispectral instrument aboard the Landsat 7 platform that is an improved version of the Thematic Mapper.

Euphotic zone – The region of the water column extending from the surface to a depth that is exposed to enough sunlight that photosynthesis can occur. Secchi disk depth is a good approximation of this area.

LD – Acronym for Lake Diefenbaker

NASA – National Aerospace and Space Administration (US Government)

Photogrammetry – A method of obtaining information from non-contact imaging. In this thesis, it refers to the analysis of photographic images to obtain data.

Radiance – A measure electromagnetic radiation that is emitted from an object that is imaged by a satellite. Typically, this measurement is in watts per steradian per square meter, but this measurement does not account for the amount of initial radiation. As such, these values are not typically used for comparisons across multiple dates

Reflectance - A unitless value that measures radiation in a way that is comparable across dates and light levels.

RMSE – Root-mean Squared error. A measure of the differences between the observed and predicted values of a model.

SDD – Acronym for Secchi disk depth

SLC – Acronym for Scan Line Corrector. A piece of equipment that corrects for orbital movement on Landsat satellites. Landsat 7's SLC failed and left all imagery with zones of lost data.

Spatial Resolution – The area represented by a single pixel on a satellite sensor. This resolution

is a 30m by 30m area for the Landsat satellites used in this study.

Spectral Bands – The number of unique intervals of the electromagnetic spectrum that a satellite can measure. The range and placement of these bands specific to each sensor, which defines its spectral resolution.

Spectral Resolution – The range of the electromagnetic spectrum that a sensor can gather data from.

SSR – Acronym for South Saskatchewan River, the primary inflow into LD

SSRB – Acronym for South Saskatchewan River Basin

Sun glint – A phenomenon common in remote sensing where the incident light reflects off rough water (often caused by waves) and unpredictably influences light detected by the satellites.

TM – Thematic Mapper, an multispectral imager aboard the Landsat 5 platform.

Temporal Resolution – The frequency a remote sensing platform can obtain another image of the same location. For Landsat satellites, the temporal resolution is 16 days.

USGS – United States Geological Survey (US Government)

Appendix B: Flood Progression 2011

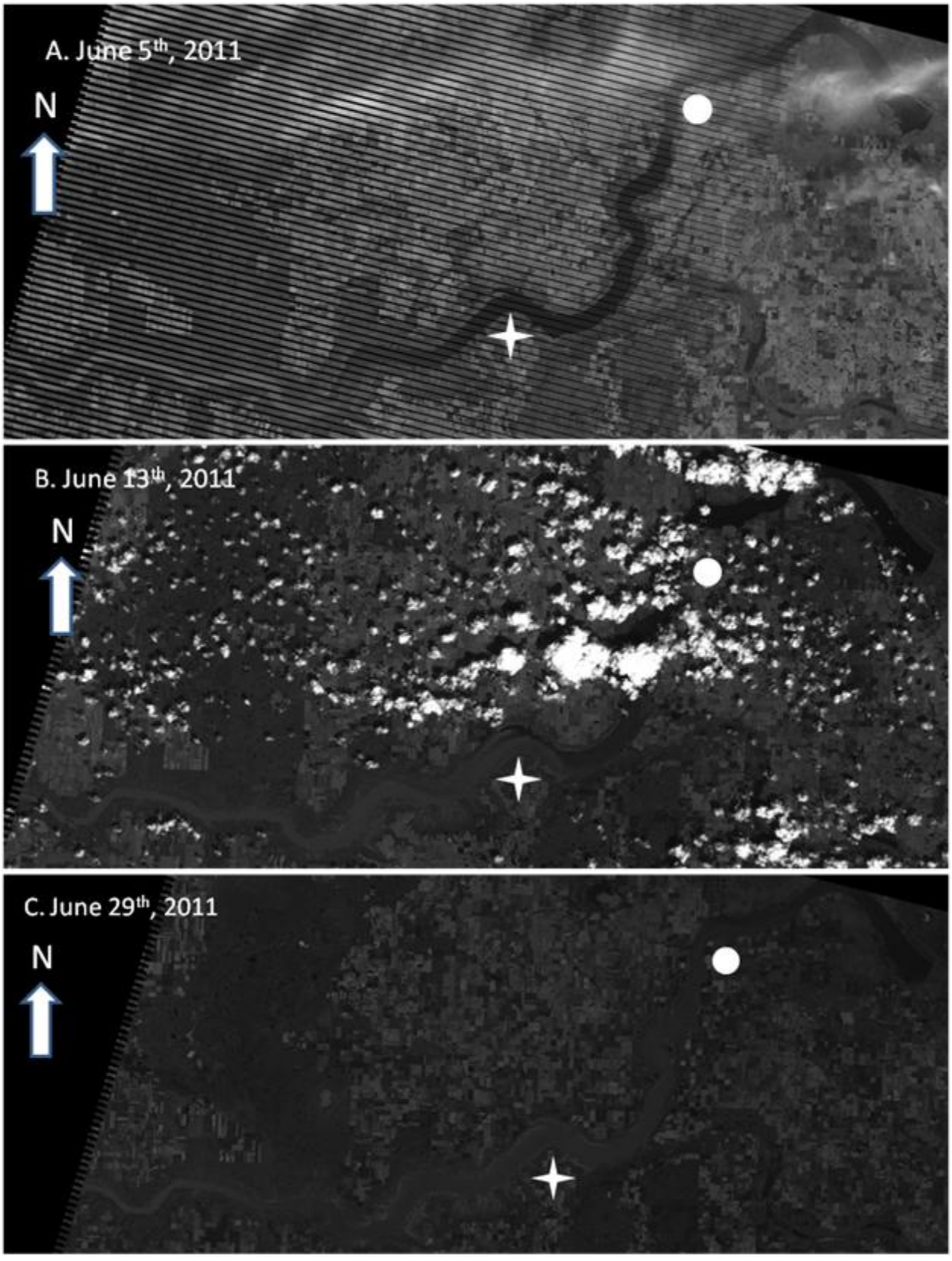

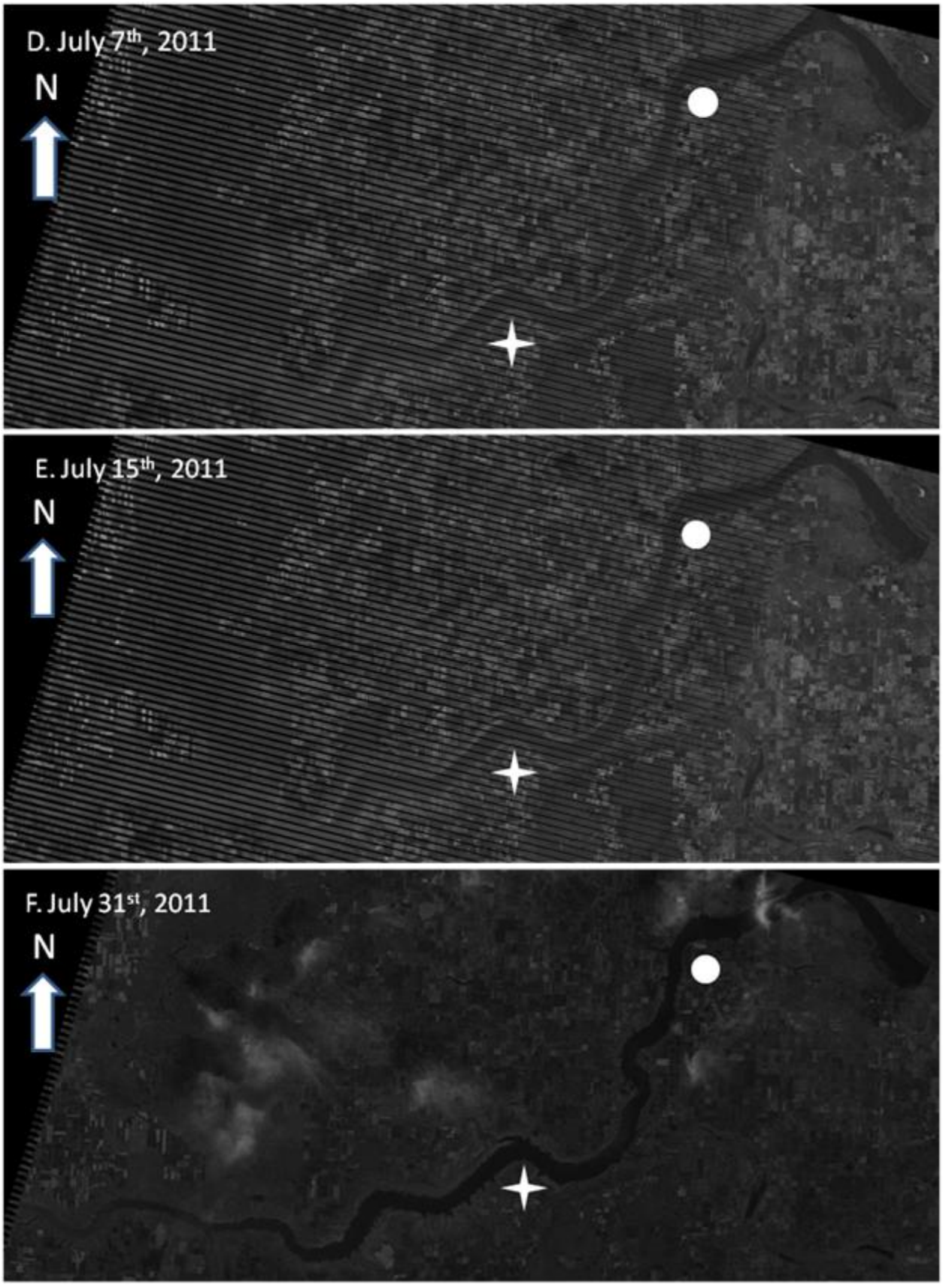
D. July 7th, 2011
N
E. July 15th, 2011
N
F. July 31st, 2011
N

These above figures are a series of Landsat 5 and 7 images taken in June and July 2011. They show the arrival and extent of a large flood event that occurred in the year. The flood arrived from the west in the SSR (A), and moved downstream (B). This flood brought high turbidity and debris, thus significantly reducing water clarity. The minimal clarity was observed at the end of June (C), before beginning to become clearer in July (D to F). Dark colored water indicated high water clarity, while grey-white water indicated low water clarity. The star is placed below a major bay, Snakebite Coulee, while the circle is placed beside Hitchcock bay further downstream. These points are placed for reference, to see how the sediment plume advances and recedes during these two months.